Check for updates

IET Control Theory & Applications

WILEY

IET The Institution of Engineering and Technology

ORIGINAL RESEARCH OPEN ACCESS

A Novel Cascaded RPIDD^2-PI Controller Tuned by Enhanced Cooperation Search Algorithm for Automatic Voltage Regulator Systems

Davut Izci[1,2] | Fatma A. Hashim[3] | Serdar Ekinci[4] | Sahar F. Sabbeh[5,6] | Mohit Bajaj[7,8] | Lukas Prokop[9] | Ievgen Zaitsev[10]

[1]Department of Electrical and Electronics Engineering, Bursa Uludag University, Bursa, Turkey | [2]Applied Science Research Center, Applied Science Private University, Amman, Jordan | [3]Faculty of Engineering, Helwan University, Helwan, Egypt | [4]Department of Computer Engineering, Bitlis Eren University, Bitlis, Turkey | [5]Department of Information Systems and Technology, College of Computer Science and Engineering, University of Jeddah, Jeddah, Saudi Arabia | [6]Faculty of Computers and Artificial Intelligence, Benha University, Benha, Egypt | [7]Department of Electrical Engineering, Graphic Era (Deemed to Be University), Dehradun, India | [8]Graphic Era Hill University, Dehradun, India | [9]ENET Centre, CEET, VSB-Technical University of Ostrava, Ostrava, Czech Republic | [10]Department of Theoretical Electrical Engineering and Diagnostics of Electrical Equipment, Institute of Electrodynamics, National Academy of Sciences of Ukraine, Kyiv, Ukraine

Correspondence: Mohit Bajaj (mohitbajaj.ee@geu.ac.in) | Ievgen Zaitsev (zaitsev@i.ua)

Received: 25 March 2025 | **Revised:** 11 August 2025 | **Accepted:** 21 August 2025

Funding:: This research is funded by European Union under the REFRESH—Research Excellence For Region Sustainability and High-Tech Industries Project via the Operational Programme Just Transition under Grant CZ.10.03.01/00/22_003/0000048; in part by the National Centre for Energy II and ExPEDite Project a Research and Innovation Action to Support the Implementation of the Climate Neutral and Smart Cities Mission Project TN02000025; and in part by ExPEDite through European Union's Horizon Mission Programme under Grant 101139527.

ABSTRACT

Voltage regulation is essential for maintaining the stability and efficiency of power systems, and automatic voltage regulators (AVRs) play a key role in ensuring consistent voltage levels and reducing disturbances. In this study, a novel cascaded controller, referred to as RPIDD^2-PI, is proposed for AVR systems, representing its first known application in literature. The controller is designed to enhance voltage regulation by improving precision, stability, and dynamic responsiveness. To optimize the controller parameters, an improved metaheuristic algorithm called the enhanced cooperation search algorithm (ECSA) has been developed. This algorithm incorporates several features, including control randomization, a linear transfer function, an adaptive *p*-best mutation strategy, and a greedy selection mechanism. These enhancements provide a balanced trade-off between exploration and exploitation during the optimization process. Simulation results show that the ECSA-tuned controller achieves excellent dynamic performance, with a rise time of 0.0314 s, a settling time of 0.0472 s, and zero overshoot, outperforming existing methods. The standard deviation of 7.9591E−05 across multiple runs highlights the consistency and robustness of the solution. Robustness tests confirm the controller's reliability under parameter uncertainties in the amplifier, exciter, and generator components, showing only minor variations in dynamic performance. Furthermore, the proposed controller demonstrates strong transient stability by minimizing oscillations and enabling a fast return to steady-state conditions. Comparative studies against more than 40 recent

Abbreviations: ARO, Artificial rabbits optimization; AVR, Automatic voltage regulator; CSA, Cooperation search algorithm; ECSA, Enhanced cooperation search algorithm; EO, Equilibrium optimizer; FOPID, Fractional-order PID; FOPIDD^2, Fractional-order PID with double derivative; GOA, Gazelle optimization algorithm; IAE, Integral of absolute error; ICA, Imperialist competitive algorithm; iRUN, Improved Runge Kutta optimizer; ISE, Integral of squared error; ITAE, Integral of time-weighted absolute error; ITSE, Integral of time-weighted squared error; L-RUN, Lévy-enhanced Runge Kutta optimizer; LTF, Linear transfer function; PDO, Prairie dog optimization; PI, Proportional-integral; PIDA, PID with acceleration; RIME, Rime optimization algorithm; RPID, Real PID; RPIDD^2, Real PID with double derivative; RUN, Runge Kutta-based optimization; SCA, Sine cosine algorithm; SMA, Slime mould algorithm; SPID, Standard PID; SPIDD^2, Standard PID with double derivative; ZLG, Dynamic response performance criteria.

This is an open access article under the terms of the Creative Commons Attribution-NonCommercial-NoDerivs License, which permits use and distribution in any medium, provided the original work is properly cited, the use is non-commercial and no modifications or adaptations are made.

© 2025 The Author(s). *IET Control Theory & Applications* published by John Wiley & Sons Ltd on behalf of The Institution of Engineering and Technology.

optimization-based controllers published between 2020 and 2023 confirm that the ECSA offers faster convergence and higher efficiency.

1 | Introduction

1.1 | Background

Automatic voltage regulators (AVRs) assume a critical role in the realm of electrical systems by upholding a stable and reliable voltage output, thereby ensuring optimal performance and safeguarding equipment against potential harm [1]. The effectiveness of an AVR hinges on its capacity to address vital parameters, encompassing voltage regulation, response time, stability, and efficiency [2]. Achieving mastery in these aspects stands as a keystone for preserving an unwavering and responsive power supply, even when confronted with varying loads and input voltages. As such, the engineering community remains ardently dedicated to exploring innovative avenues for augmenting AVR control methodologies [3–5].

Employing a controller alongside an AVR holds immense significance for several compelling reasons. Primarily, a controller furnishes a centralized system for vigilant monitoring and regulation of the AVR, ushering in heightened efficiency and efficacy in voltage control. This controller becomes the hub for accumulating critical data on voltage, frequency, and other system parameters, which it leverages to make real-time adjustments to the AVR, thereby upholding voltage stability. Second, a controller introduces advanced capabilities, including remote monitoring, fault detection, and automatic shutdown during emergencies, thus serving as a bulwark against equipment damage, minimizing downtime, ensuring personnel safety and providing resilience. Last, a controller elevates system reliability and performance by delivering instantaneous feedback and control over the AVR. This, in turn, aids in optimizing the generator or alternator's efficiency, curtailing energy consumption, and prolonging equipment lifespan. Consequently, an array of controllers finds application in this context, spanning from the standard proportional integral-derivative (SPID) [6], to the real PID (RPID) [7], PID acceleration (PIDA) [8], fractional-order PID (FOPID) [9], SPID with second-order derivative (SPIDD^2) [10], and FOPID with double-derivative (FOPIDD^2) [11]. Each of these controllers brings its unique attributes to the table, catering to diverse needs in the realm of AVR control and regulation.

1.2 | Literature

In the relevant literature, one can see SPID, RPID, FOPID and SPIDD^2 controllers as widely adopted typical controllers in AVR system. The SPID controller is a widely used control system. It comprises three key components: the proportional (K_p), integral (K_i), and derivative (K_d) gains, which are combined to determine the control signal. The transfer function for SPID is defined as follows [12].

$$C_{SPID}\ (s) = K_p + \frac{K_i}{s} + K_d s \tag{1}$$

The RPID controller is a variation of the SPID controller that incorporates a modification to the derivative term. It introduces additional filter coefficient, N, enhancing control flexibility. The transfer function for RPID is expressed as follows [13].

$$C_{RPID}\ (s) = K_p + \frac{K_i}{s} + K_d \frac{Ns}{s+N} \tag{2}$$

FOPID controllers offer a more flexible approach by introducing fractional orders (λ and μ) to the integral and derivative terms [14]. This allows for control customization based on the specific system's requirements. The FOPID transfer function is given by Equation (3) [15].

$$C_{FOPID}\ (s) = K_p + \frac{K_i}{s^\lambda} + K_d s^\mu \tag{3}$$

The SPIDD^2 controller is also an extension of the SPID controller that introduces a second-order derivative term. This added complexity enhances the controller's ability to address certain system dynamics. The SPIDD^2 controller's transfer function is defined as follows [16].

$$C_{SPIDD^2}\ (s) = K_p + \frac{K_i}{s} + K_{d1} s + K_{d2} s^2 \tag{4}$$

Each of these controllers offers distinct advantages and characteristics, making them suitable for AVR control applications. It is worth noting that different controller structures have also been adopted, as presented in Table 1; however we specifically attempt to provide a brief definition for widely adopted ones. Apart from the control structures, the cost function being adopted has also significant effect on the performance. To get the most favorable control method, the researchers have employed different cost functions, as well. In terms of cost functions, well-established error-based performance indices known as integral of time-weighted squared error (ITSE), integral of squared error (ISE), the integral of absolute error (IAE) and integral of time-weighted absolute error (ITAE) along with dynamic response performance criteria based ZLG have been adopted in AVR related studies. The definition of ZLG performance index is given in Equation (5) [17]:

$$ZLG = (1-\sigma)\ \cdot \left(M_p + E_{ss}\right) + \sigma \cdot (ST - RT) \tag{5}$$

where σ is weighting factor and σ is set to $e^{-1} = 0.3679$. Equations (6), (7), (8) and (9) provide the definitions for IAE, ISE, ITAE and ITSE performance indices, respectively [44].

$$IAE = \int_0^{t_f} \left|V_t - V_{ref}\right| \cdot dt \tag{6}$$

$$ISE = \int_0^{t_f} \left(V_t - V_{ref}\right)^2 \cdot dt \tag{7}$$

17518652, 2025, 1, Downloaded from https://ietresearch.onlinelibrary.wiley.com/doi/10.1049/cth2.70068 by Bursa Uludag University Kutuphane ve Dokumantasyon, Wiley Online Library on [07/09/2026]. See the Terms and Conditions (https://onlinelibrary.wiley.com/terms-and-conditions) on Wiley Online Library for rules of use; OA articles are governed by the applicable Creative Commons License

TABLE 1 | Recently reported effective methods, including controller type, optimizer and cost function for AVR system control.

Ref.	Year	Controller type	Optimizer	Cost function
[18]	2019	SPID	SCA	ZLG
[19]	2020		TSA	ITSE
[20]	2022		L-RSANM	ZLG
[21]	2023		EWOA	ITAE
[9]	2022	FOPID	ChBWO	Combination of ZLG and ITAE
[22]	2023		IGBO	ITAE
[23]	2023		MGWO	Combination of ITAE and ITSE
[24]	2022		MSFA	ZLG
[25]	2021	SPID, RPID, FOPID and SPIDD^2	SA-MRFO	Modified version of ZLG
[26]	2022	RPID	SOS	ZLG
[7]	2022	SPID, RPID, FOPID and SPIDD^2	AOA	ZLG
[27]	2023	SPIDD^2	L-RUN	ISE
[28]	2023	SPIDD^2	enAO	Modified version of ITSE
[29]	2022	SPID, RPID, FOPID and SPIDD^2	FDB-LFD	Modified version of ZLG and ITAE
[30]	2023	TI$^\lambda$DND^{2}N^2	EO	ZLG
[31]	2021	Resilient PID	GA	Modified version of ZLG
[32]	2022	MFOPID	Rao	IAE, ISE, ITAE and ITSE
[33]	2021	FOPIDFF	SCA	ZLG
[34]	2020	2DOF state feedback PI	PSO	Simple cost function
[35]	2019	HODFC and FHODFC	PSO	Modified version of ITAE
[36]	2022	Sigmoid PID	NSCA	Modified version of ZLG
[37]	2022	Fuzzy PID	GA	Modified version of ITAE
[38]	2016	Gray PID	ICA	ZLG
[39]	2021	FOPID-DN	EO	IAE, ISE, ITAE and ITSE
[40]	2022	FOPID and PI$^\lambda$DND^{2}N^2	COA	Modified version of ITAE
[41]	2019	NN predictive	ICA	ITAE
[11]	2023	SPID, FOPID, SPIDD^2 and FOPIDD^2	RSA	ZLG
[42]	2019	SPID and PIDA	WOA	ISE
[43]	2022	RPIDD^2	iRUN	ZLG

$$ITAE = \int_0^{t_f} t \cdot \left| V_t - V_{ref} \right| \cdot dt \tag{8}$$

$$ITSE = \int_0^{t_f} t \cdot \left(V_t - V_{ref} \right)^2 \cdot dt \tag{9}$$

In the definitions given above, t_f denotes the final simulation time, V_t is the terminal voltage and V_{ref} is the reference voltage. Table 1 lists recently reported (between 2020 and 2023) works along with their respective controller types, optimizers, and cost functions. The readers are referred to the reported studies in [45–63] for various AVR studies from 2024. As can be seen, interest in the topic of AVR control continues to grow steadily.

1.3 | Limitations and Motivations

In a power system, the AVR plays an indispensable role in safeguarding voltage stability and ensuring that connected electrical equipment operates within acceptable voltage limits [64]. The absence of proper voltage regulation can lead to severe consequences, including equipment damage, operational failures, costly downtime, and the need for extensive repairs. Consequently, the AVR stands as a linchpin in power systems reliant on generators or alternators for electricity generation. While existing control methodologies, as outlined in Table 1, have demonstrated success to a certain degree, they are not without their limitations. Notably, issues related to robustness, relatively higher overshoots, prolonged rise, settling, and peak times, as well as persistent steady-state errors, persist in these existing control approaches. It is these very challenges that underscore the motivation for our study. Therefore, the primary motivation behind this research

17518652, 2025, 1, Downloaded from https://ietresearch.onlinelibrary.wiley.com/doi/10.1049/cth2.70068 by Bursa Uludag University Kutuphane ve Dokumantasyon, Wiley Online Library on [07/09/2026]. See the Terms and Conditions (https://onlinelibrary.wiley.com/terms-and-conditions) on Wiley Online Library for rules of use; OA articles are governed by the applicable Creative Commons License

is to propose a more advanced control scheme that can effectively address the aforementioned limitations. Furthermore, as part of our motivation, we have developed a novel optimizer based on the cooperation search algorithm (CSA) [65] for fine-tuning the parameters of our proposed control scheme, thereby improving its overall performance and adaptability. Together, these efforts aim to push the boundaries of AVR control and contribute to the development of more robust and efficient power systems.

1.4 | Main Contributions

In pursuit of the motivations presented in previous section, we introduce a novel cascaded RPIDD^2-PI controller, which serves as an innovative alternative to the existing array of controller types. This controller configuration is designed to offer enhanced precision, stability, and responsiveness in voltage regulation, mitigating the shortcomings associated with conventional methods. It is also worth noting that this is the first study that reports the implementation of such a controller scheme for the AVR system. Besides, an enhanced cooperation search algorithm (ECSA) has also been developed as a novel optimizer as part of the motivation of this work. The proposed ECSA uses control randomization, linear transfer function, new exploration, and exploitation stages along with greedy selection strategy for increased performance. This optimizer is instrumental in fine-tuning the parameters of our proposed control scheme, thereby improving its overall performance and adaptability. The ZLG cost function is also used for minimization which is advantageous because it effectively minimizes dynamic response performance criteria, including maximum overshoot, steady-state error, settling time, and rise time. This ensures that the AVR system meets stringent performance requirements. Therefore, this paper focuses on demonstrating the superior performance of the proposed cascaded RPIDD^2-PI controller, tuned via novel ECSA optimizer, in addressing the aforementioned challenges of AVR control. This method aims to surpass other reported AVR control techniques in terms of stability, speed of response, robustness, and efficiency. Considering those innovations, the main contributions of this study can be listed as follows. In the subsequent sections, we delve into the intricacies of our proposed control scheme, its components, implementation, and the results of its application in addressing the identified limitations and enhancing the performance of AVR systems.

1.5 | Organization of Study

This paper is organized as follows. Section 2 introduces the original CSA while Section 3 delves into the proposed ECSA, highlighting its improvements. Section 4 focuses on AVR system modeling and the properties of the uncontrolled system. Section 5 presents a novel design procedure using the ECSA-based cascaded RPIDD^2-PI controller. Section 6 contains simulation results and the validation of the proposed approach, including statistical validation of ECSA, convergence analysis, transient stability evaluation, robustness analysis, and comparisons with various controller types. The latter section also offers a discussion of the research outcomes and implications. Section 7 concludes the paper by summarizing the key findings and the significance of the ECSA-based approach in AVR system control.

2 | Cooperation Search Algorithm

Population-based metaheuristic cooperation search algorithm (CSA) [65] replicates social community cooperation. CSA is popular because it can solve many optimization problems and find high-quality solutions. CSA employs agents who may solve the optimization problem. These agents collaborate to search the space and find optimal or near-optimal solutions. Main CSA components include agent initialization, cooperation, exploitation, and termination criteria. Initial agents represent potential problem solutions and are randomly produced. The search space position of each agent is determined by its choice factors. Cooperation, where agents share knowledge to enhance their solutions, is fundamental to CSA. This information exchange is usually done cooperatively by sharing best solutions, promising search directions, or beneficial knowledge. Cooperation increases population diversity and allows search space expansion. The exploitation phase refines solutions using cooperation-gained knowledge. Local search operations allow agents to exploit potential search space regions and refine their solutions to optimal or near-optimal solutions. CSA repeats collaboration and exploitation until a termination requirement is fulfilled. The termination criterion can be a maximum iteration count, fitness value, or computing time restriction. After meeting the termination requirement, the algorithm gives the best search result. The CSA algorithm is described below.

2.1 | Teamwork Formation

During the teamwork formation stage, all team members (solutions) are initialized randomly. Each team member represents a possible solution to the optimization problem. The initialization process involves assigning random values to the parameters or variables that define each solution. This random initialization ensures a diverse starting point for the optimization process. The function *Ψ(LB, UB)* generates a uniformly distributed random number between the lower bound (LB) and the upper bound (UB). This function is used to initialize the parameter values in the solutions randomly. Equation (10) is used to initialize all team members randomly and to create random pairings of parameter values from different solutions within the population. These pairings are essential for the subsequent stages of cooperation search, where cooperation and information sharing among the solutions take place.

$$x_{i,j}^{k} = \psi\left(x_i, x_j\right),\ i \in [1, I], j \in [1, J], k = 1 \tag{10}$$

where $x_{i,j}^{k}$ represents the value of the j^{th} parameter of the i^{th} solution at the k^{th} cycle. I is size of the population or the number of individuals being considered at a given cycle, J is the total number of parameters in each solution—the dimensionality of the search space—and k is the cycle number or iteration count of the optimization process. (x_i, x_j) represents the formation of a pair of parameter values from two different solutions. This pairing is performed for each parameter (j) and each solution (i) within the population.

17518652, 2025, 1, Downloaded from https://ietresearch.onlinelibrary.wiley.com/doi/10.1049/cth2.70068 by Bursa Uludag University Kutuphane ve Dokumantasyon, Wiley Online Library on [07/09/2026]. See the Terms and Conditions (https://onlinelibrary.wiley.com/terms-and-conditions) on Wiley Online Library for rules of use; OA articles are governed by the applicable Creative Commons License

2.2 | Teamwork Cooperation

This stage involves sharing knowledge among the team members, including the chairman, supervisors, and directors. The teamwork communication includes three types of knowledge: The chairman's knowledge (C), the knowledge of the board of directors (D), and the board of supervisors' knowledge (S).

- **Chairman's Knowledge**: The chairman's knowledge (C) represents the expertise or information possessed by the randomly selected chairman from the directors' board. The chairman is chosen through a random selection process to simulate the rotation process. This implies that the role of the chairman is not fixed but changes among the directors over time.
- **Board of Directors' Knowledge**: The knowledge of the board of directors (D) refers to the collective knowledge held by all the directors. Each director contributes their knowledge to the pool of information available for cooperation. The directors hold an equal position in computing and sharing this knowledge.
- **Board of Supervisors' Knowledge**: Similarly, the board of supervisors' knowledge (S) represents the combined knowledge of all the supervisors. The supervisors also have an equal position in contributing to the knowledge pool and sharing information.

Each member can acquire additional knowledge with the chairman, supervisors and directors, as shown in Equation (11). The chairman is randomly selected from the directors' board to simulate the rotation process, whereas all the directors and supervisors are given an equal position in computing D and S.

$$u_{i,j}^{k+1} = X_{i,j}^{k} + C_{i,j}^{k} + D_{i,j}^{k} + S_{i,j}^{k},\ i \in [1, I],\ j \in [1, J],\ k \in [1, K] \quad (11)$$

where $u_{i,j}^{k+1}$ is the j^{th} value of the i^{th} group solution at the $(k+1)^{th}$ iteration. It is the summation of the current solution $X_{i,j}^{k}$ with the knowledge acquired from $C_{i,j}^{k}$, $D_{i,j}^{k}$, and $S_{i,j}^{k}$. These parameters are calculated using Equations (12), (13), and (14), respectively.

$$C_{i,j}^{k} = log\left(\frac{1}{\Phi(0,1)}\right) \cdot \left(glBest_{indx,j}^{k} - x_{i,j}^{k}\right) \quad (12)$$

where $C_{i,j}^{k}$ is the knowledge gained from the chairman randomly chosen from the best-known global solution $glBest_{indx,j}^{k}$, where indx is a randomly chosen index from $[1,\ 2, .., M]$.

$$D_{i,j}^{k} = \alpha \cdot \phi(0,1)\left[\frac{1}{M}\sum_{m=1}^{M} glBest_{m,j}^{k} - X_{i,j}^{k}\right] \quad (13)$$

where $D_{i,j}^{k}$ represents the gained knowledge from the board of directors chosen from the M best-known global learnt solutions. It is calculated by averaging the differences between the j^{th} value of the i^{th} group solution $X_{i,j}^{k}$ and the j^{th} value of the m^{th} best-known global solution $glBest_{m,j}^{k}$, where m ranges from 1 to M.

$$S_{i,j}^{k} = \alpha - \phi(0,1)\left[\frac{1}{I}\sum_{m=1}^{M} perBest_{m,j}^{k} - X_{i,j}^{k}\right] \quad (14)$$

where: $S_{i,j}^{k}$ is the knowledge gained from the supervisors randomly chosen from the external selected set. It is calculated as the average of the differences between the j^{th} value of the i^{th} group solution $X_{i,j}^{k}$ and the j^{th} value of the m^{th} personal best-known solution per $Best_{m,j}^{k}$, where m ranges from 1 to $(M-1)$. The values of (C), (D), and (S) are scaled by the learning coefficient ϕ and a random variable generated using the standard normal distribution $\phi(0,1)$.

2.3 | Exploitation

Besides gaining knowledge from the leaders' solutions, members can similarly acquire knowledge by summing their own experiences and retaining their in-memory information, as shown below:

$$v_{i,j}^{k+1} = \begin{cases} r_{ij}^{k+1} & if\ \left(u_{ij}^{k+1} \geq c_j\right) \\ p_{i,j}^{k+1} & if\ \left(u_{i,j}^{k+1} < c_j\right) \end{cases},\ i \in [1, I],\ j \in [1, J],\ k \in [1, K] \quad (15)$$

$$r_{ij}^{k+1} = \begin{cases} \phi\left(\overset{\%}{x}_j + \underset{-j}{x} - u_{ij}^{k+1}, c + j\right) & if\ \left(\left|u_{i,j}^{k+1} - c_j\right| < \phi(0,1) \cdot \left|\bar{x}_j - \underset{-j}{x}\right|\right) \\ \phi\left(x_j, \bar{x}_j + x_j - u_{i,j}^{k+1}\right) & Otherwise \end{cases} \quad (16)$$

$$p_{i,j}^{k+1} = \begin{cases} \phi\left(c_j, \bar{x}_j + \underset{-j}{x} - u_{i,j}^{k+1}\right) \\ \phi\left(\bar{x}_j + \underset{-j}{x} - u_{i,j}^{k+1}, \bar{x}_j\right) \end{cases} if\ \left(\left|u_{i,j}^{k+1} - c_j\right| < \phi(0,1) \cdot \left|\bar{x}_j - \underset{-j}{x}\right|\right) \quad (17)$$

$$c_j = \left(\bar{x}_j + \underset{-i}{x}\right) \cdot 0.5 \quad (18)$$

where v_{ij}^{k+1} represents the j^{th} value of i^{th} reflective solution at the $(k+1)^{\text{th}}$ iteration. The team slowly improves its competitiveness by ensuring the attainment of all the team members with superior performance as follows:

$$x_{i,j}^{k+1} = \begin{cases} u_{i,j}^{k+1}\ if\ \left(F\left(u_i^{k+1}\right) \leq F\left(v_i^{k+1}\right)\right) \\ v_{i,j}^{k+1}\ if (F\left(u_i^{k+1}\right) > F\left(v_i^{k+1}\right)) \end{cases},$$
$$i \in [1, I],\ j \in [1, J],\ k \in [1, K] \quad (19)$$

where $F(x)$ is the fitness value of solution x. A number of restrictions are employed, and the initial step is to utilize Equation (20) to bring all of the variables in solution into the feasible zone. Next, we take the objective value $F(x)$ and the value of the constraint violation and use the penalty functions in Equation (21) to get the fitness value $F(x)$. After then, the exercise value is equivalent to the goal value, and all limitations are clearly defined for the workable options. To make the fitness value greater than the objective value, the constraint violation value is set to positive for

17518652, 2025, 1, Downloaded from https://ietresearch.onlinelibrary.wiley.com/doi/10.1049/cit2.70068 by Bursa Uludag University Kutuphane ve Dokumantasyon, Wiley Online Library on [07/09/2026]. See the Terms and Conditions (https://onlinelibrary.wiley.com/terms-and-conditions) on Wiley Online Library for rules of use; OA articles are governed by the applicable Creative Commons License

the infeasible options. This allows the group to be directed to a search region that is both possible and worth exploring.

$$x_j = \max\left\{\min\left\{\bar{x}_j, x_j\right\}, \underline{x}_j\right\} \tag{20}$$

$$F(x) = f(x) + \sum_{k=1}^{E} c_e^1 \cdot \max\{g_e(x), 0\} + \sum_{f=1}^{E} c_f^2 \cdot \left|h_f(x)\right| \tag{21}$$

where x_j is the j^{th} value of the x solution to be evaluated. c_e^1, c_f^2 are the coefficients of penalty for the e^{th}, and the f^{th} inequality constraint, respectively.

3 | Enhanced Cooperation Search Algorithm

This section presents the proposed enhanced CSA (ECSA) optimization method. The section begins with a study of the inadequacies of the original CSA, followed by the design of the proposed ECSA, which evolves the initial population of the problem solution.

3.1 | Limitations of the Original Algorithm

Here are a few areas where the CSA algorithm falls short. The local optimum may occur if the capacity to guarantee a balanced transition between exploration and exploitation is inadequate. The CSA's movement step value is core-based and fixed across all iterations, making global exploration and local exploitation difficult. In order to facilitate rapid solution discovery and avoid undesirable search spaces, no selection is applied.

3.2 | Architecture of the ECSA Algorithm

The limitations of the CSA motivated the development of the ECSA. In the ECSA, performance is boosted using four main approaches:

- Control randomization operator.
- Linear transfer function.
- Exploration–exploitation based on adaptive p-best mutation.
- Greedy selection strategy.

3.2.1 | First Approach: Control Randomization

The ECSA uses a control randomization operator (Ran) to select a new position in the direction of the best solution. Random values enable exploring new positions in different directions and reduce the probability of being stuck in the local optima or premature convergence. Ran is used to modify Equation (23) as follows:

$$C_{i,j}^k = \log\left(\frac{1}{\Phi(0,1)}\right) \cdot \text{Ran} \cdot \left(glBest_{indx,j}^k - x_{i,j}^k\right) \tag{22}$$

where the Ran operator is given by:

$$\text{Ran} = 2 \cdot \text{rand} - 1 \tag{23}$$

3.2.2 | Second Approach: Linear Transfer Function

A linear transfer function (LTF) is used to enable the gradual transfer of the algorithm from exploration to exploitation. It is well known that the balance between the global search (exploration) and the local search (exploitation) is crucial for the algorithm's performance. Thus, the ECSA uses the LTF to balance exploration and exploitation, as strong exploration should be performed during the first steps. In contrast, exploitation should be maximized during the last steps to find the best results. The LTF is given by:

$$LTF = exp\left(-\frac{t}{T_{max}}\right) \tag{24}$$

The LTF is used during the new adaptive p-mutation-based exploration–exploitation phase.

3.2.3 | Third Approach: New Exploration–Exploitation Stage

A new exploration–exploitation stage based on adaptive p-best mutation. The adaptive p-best mutation algorithm enables transitioning gradually from exploration to exploitation during iterations. The strategy uses a mutation operator and utilizes several top solutions in mutation rather than the best one. It produces a mutant vector y as follows:

$$y = x_{pbest} + F(x_{r2} - x_{r3}) \tag{25}$$

where: x_{pbest} is randomly chosen from the top solution set $p \times NP$ ($p \in [0, 1]$). The value of p significantly impacts the achievement of exploration and exploitation balance. A small p-value may result in fast and high probability premature convergence. In this study, the p-value is gradually changed during the search by a linear decreasing rule as follows:

$$p(t) = 1 - \left(1 - \frac{1}{NP}\right) \cdot \frac{t-1}{T_{\max} - 1} \tag{26}$$

where t is the t^{th} iteration, $T_{\max}$ is the number of maximum iterations allowed, NP Is the number of individuals in the population. Thus, large values of p enable global exploration in the early iterations. However, during the later iterations, small values of p are used to enable better local exploitation to accelerate the convergence speed. In particular, when t = 1 (i.e., $p = 1$), the mutation operator ' DE/rand/1 ' is utilized; when $t = T_{max}$ (i.e., $p = 1/\text{NP}$), the ' DE/ best /1 ' is applied. A mutant vector y is produced for each target vector x_k using the directional mutation rule in which scaled directed differential variation is multiplied by a 'directed' Factor d. Additionally, the LTF is injected in this phase to enable better exploration–exploitation, as follows:

$$y = x_{pbest} + d \cdot F(x_{r2} - x_{r3}) \cdot LTF \tag{27}$$

where: d is either 1 or −1 based on the relation between the difference vectors x_{r2} and x_{r3} as follows:

$$d = \begin{cases} 1 & \text{if } x_{r2} \text{ is better than } x_{r3} \\ -1 & \text{otherwise} \end{cases} \tag{28}$$

17518652, 2025, 1, Downloaded from https://ietresearch.onlinelibrary.wiley.com/doi/10.1049/cth2.70068 by Bursa Uludag University Kutuphane ve Dokumantasyon, Wiley Online Library on [07/09/2026]. See the Terms and Conditions (https://onlinelibrary.wiley.com/terms-and-conditions) on Wiley Online Library for rules of use; OA articles are governed by the applicable Creative Commons License

Algorithm 1 | The Proposed ECSA Algorithm

```
Input: Objective function, constraints, maximum number of iterations
Output: Final solution (global best-known solution)
procedure OPTIMIZE ()
iter ← 1
swarm ← generate initial swarm using Equation (10)
fitness ← evaluate fitness using Equation (21)
group ← swarm
reflective ← swarm
  while iter ≤ max_iterations do
    for each individual in swarm do
      y ← generate mutant vector using adaptive p-best mutation
      y ← apply Equations (22)–(28) to refine mutant vector
      update personal best solution (I)
      update global best solution (M)
      global_exploit ← apply Equations (11), (26), (13), (14)
      local_explore ← apply Equations (15)–(18)
      evaluate fitness of all solutions using Equation (21)
      select better solutions using Equation (19)
      iter ← iter + 1
    end for
  apply greedy selection between current and previous solutions
end while
return global best-known solution
```

This rule guarantees that the differential variation is oriented toward a better vector, thus increasing the possibility of creating an improved solution.

3.2.4 | Fourth Approach: Greedy Selection Strategy

Finally, ECSA utilizes a greedy selection strategy between the generated and current solutions to reject the poorly generated solutions and avoid deviation from existing promising zones. Algorithm 1 provides the pseudocode of the proposed ECSA algorithm.

3.3 | Performance Evaluation of the ECSA on CEC Functions

The CEC2020's benchmark functions were used to evaluate the performance of the ECSA. Table 2 shows the performance scores of the experimented algorithms in terms of the min/best, max/worst, mean, and standard deviation (Std) of the fitness score. Results show that the ECSA achieved the best mean in eight functions (F2, F3, F4, F5, F6, F7, F8, and F9), outperformed its competitors in terms of all metrics in five functions (F3, F4, F6, F8, and F9). However, CGO outperformed the performance of all the algorithms in (F1, F5, and F7) besides achieving the best mean for F10. Consequently, we can conclude that ECSA has good stability and search capabilities compared to the baseline algorithms.

For more analysis, the Wilcoxon sum-rank test was conducted to evaluate how much ECSA and its competitors differ. The Wilcoxon test is a non-parametric statistical test that compares two paired algorithms to determine whether their performance scores are significantly different based on the p-value. The Wilcoxon scores in Table 3 indicate that ECSA and the original CSA have a high p-value in F2, F7, and F8, which indicates the similar performance of the two algorithms. Moreover, ECSA has a high similarity score with HHO in F10, PSO in F7, SSA in (F5 and F7), and GTO in (F1 and F10). However, ECSA differs highly from CGO, WOA, and TSA in all functions. Finally, ECSA has a low p-value among all the competitors for F3, F4, F6, and F9.

To further confirm the previous results, the Friedman test was used to compare and evaluate the sum of the ranks of the scores to identify changes over time. Friedman test ranks algorithms based on their performance scores; the smaller the ranking, the better the algorithm's performance. The results in Table 4 indicate that ECSA has both the lowest Friedman's mean and the mean rank, implying that ECSA performs better than its competitors.

4 | AVR System Modeling and Properties of Uncontrolled System

An AVR is a crucial device in power systems, responsible for controlling and stabilizing the generator's output voltage. Its primary function is to ensure a consistent output voltage, even when the load or input voltage fluctuates [11]. To achieve this, the AVR continually receives signals from the generator's output voltage, compares them to a reference voltage, and adjusts the alternator's field current (shown in Figure 1) accordingly. This regulation process relies on various electronic components like amplifiers, exciters, generators, and sensors, each with their respective transfer functions and operational ranges, as shown in Figure 1 [66]. In order to present a fair assessment comparatively with the reported literature (see references listed in Table 1), the gain and time constants of the amplifier, exciter, generator, and sensor have been chosen as $K_a = 10$, $T_a = 0.1$ s, $K_e = 1.0$, $T_e = 0.4$ s, $K_g = 1.0$ and $T_g = 1.0$ s, $K_s = 1.0$ and $T_s = 0.01$ s. Using those values together with the linearized model depicted in Figure 1, the transfer function provided in Equation (29) can be obtained for an AVR system with no control.

$$T_{no-control}(s) = \frac{0.1s + 10}{0.0004s^4 + 0.0454s^3 + 0.555s^2 + 1.51s + 11} \tag{29}$$

With the employment of an uncontrolled AVR system, the step response of the system presented in Figure 2, can be obtained. As seen from the respective illustration, the response is highly oscillatory at the beginning which may lead to catastrophic failures given the high voltages in a power system. Therefore, an appropriate controller is necessary to tackle any undesirable failures.

17518652, 2025, 1, Downloaded from https://ietresearch.onlinelibrary.wiley.com/doi/10.1049/cth2.70068 by Bursa Uludag University Kutuphane ve Dokumantasyon, Wiley Online Library on [07/09/2026]. See the Terms and Conditions (https://onlinelibrary.wiley.com/terms-and-conditions) on Wiley Online Library for rules of use; OA articles are governed by the applicable Creative Commons License

TABLE 2 | The fitness score results of CEC2020 functions.

F_No	Metric	ECSA	CSA	CGO	HHO	SSA	GTO	WOA	PSO	TSA
F1	min	1.04E+02	1.10E+02	1.00E+02	2.91E+03	2.90E+03	1.03E+02	1.46E+07	2.90E+03	2.98E+03
	max	7.65E+03	1.21E+04	2.63E+02	3.01E+03	3.00E+03	8.33E+03	7.19E+07	3.00E+03	5.03E+03
	mean	1.56E+03	3.61E+03	1.19E+02	2.98E+03	2.95E+03	1.76E+03	3.05E+07	2.96E+03	3.53E+03
	std	1.88E+03	3.90E+03	3.83E+01	2.51E+01	3.21E+01	2.36E+03	1.64E+07	3.17E+01	4.74E+02
F2	min	1.25E+03	1.46E+03	1.78E+03	2.04E+03	2.73E+03	2.12E+03	2.49E+03	1.90E+03	2.76E+03
	max	4.97E+03	2.79E+03	3.67E+03	3.83E+03	5.32E+03	4.19E+03	5.08E+03	3.75E+03	5.70E+03
	mean	2.07E+03	2.07E+03	2.60E+03	2.90E+03	3.58E+03	3.19E+03	3.74E+03	2.68E+03	4.03E+03
	std	6.48E+02	3.81E+02	5.37E+02	4.64E+02	5.92E+02	5.70E+02	5.93E+02	4.65E+02	6.41E+02
F3	min	7.27E+02	7.39E+02	1.78E+03	8.35E+02	7.38E+02	7.94E+02	8.46E+02	7.41E+02	8.74E+02
	max	7.47E+02	7.98E+02	3.67E+03	9.71E+02	9.07E+02	9.18E+02	1.04E+03	7.79E+02	1.04E+03
	mean	7.33E+02	7.62E+02	2.60E+03	9.00E+02	8.06E+02	8.42E+02	9.57E+02	7.59E+02	9.49E+02
	std	5.21E+00	1.14E+01	5.37E+02	3.01E+01	3.74E+01	3.00E+01	4.48E+01	1.12E+01	4.10E+01
F4	min	1.90E+03	1.90E+03	1.90E+03	1.91E+03	1.90E+03	1.90E+03	1.92E+03	1.90E+03	2.12E+03
	max	1.90E+03	1.91E+03	1.91E+03	1.93E+03	1.91E+03	1.94E+03	2.08E+03	1.91E+03	6.59E+05
	mean	1.90E+03	1.90E+03	1.90E+03	1.92E+03	1.90E+03	1.91E+03	1.95E+03	1.90E+03	1.01E+05
	std	5.81E-01	1.38E+00	1.54E+00	5.26E+00	1.69E+00	7.75E+00	3.70E+01	8.86E-01	1.67E+05
F5	min	7.62E+04	7.54E+04	2.34E+03	4.57E+04	1.09E+04	2.61E+03	7.20E+04	1.95E+04	9.97E+04
	max	3.08E+05	2.99E+05	5.79E+03	2.21E+06	6.93E+05	1.87E+04	5.03E+06	2.59E+05	4.89E+06
	mean	1.91E+05	1.28E+05	3.34E+03	5.81E+05	2.05E+05	6.91E+03	1.20E+06	9.96E+04	1.61E+06
	std	6.95E+04	4.02E+04	7.90E+02	4.48E+05	1.76E+05	4.02E+03	1.02E+06	6.06E+04	1.36E+06
F6	min	1.60E+03	1.62E+03	1.61E+03	1.78E+03	1.70E+03	1.61E+03	1.79E+03	1.72E+03	2.15E+03
	max	1.74E+03	2.26E+03	2.33E+03	2.72E+03	2.53E+03	2.51E+03	2.99E+03	2.26E+03	2.79E+03
	mean	1.62E+03	1.85E+03	1.88E+03	2.16E+03	2.13E+03	1.91E+03	2.42E+03	1.93E+03	2.45E+03
	std	2.50E+01	1.61E+02	1.77E+02	2.12E+02	2.12E+02	1.97E+02	2.91E+02	1.31E+02	1.93E+02
F7	min	8.16E+03	5.14E+03	2.36E+03	6.15E+04	6.54E+03	2.54E+03	1.01E+04	4.68E+03	1.41E+04
	max	2.77E+05	3.29E+05	3.34E+03	8.26E+05	5.27E+05	1.27E+04	3.58E+06	3.13E+05	1.12E+07
	mean	1.14E+05	9.71E+04	2.84E+03	2.42E+05	8.87E+04	4.31E+03	1.01E+06	8.92E+04	1.29E+06
	std	7.66E+04	7.50E+04	2.67E+02	1.75E+05	1.04E+05	1.94E+03	9.80E+05	7.95E+04	2.36E+06
F8	min	2.30E+03	2.30E+03	2.30E+03	2.31E+03	2.30E+03	2.30E+03	2.32E+03	2.30E+03	2.43E+03
	max	2.30E+03	2.30E+03	2.31E+03	6.08E+03	5.51E+03	5.97E+03	6.73E+03	5.98E+03	6.55E+03
	mean	2.30E+03	2.30E+03	2.30E+03	4.06E+03	2.91E+03	2.42E+03	3.96E+03	3.20E+03	4.74E+03
	std	7.99E-01	6.97E-01	1.32E+00	1.59E+03	1.07E+03	6.70E+02	1.70E+03	1.33E+03	1.42E+03
F9	min	2.80E+03	2.82E+03	2.81E+03	2.92E+03	2.82E+03	2.84E+03	2.90E+03	2.83E+03	2.95E+03
	max	2.83E+03	2.86E+03	2.93E+03	3.33E+03	2.91E+03	3.03E+03	3.09E+03	2.92E+03	3.24E+03
	mean	2.81E+03	2.84E+03	2.85E+03	3.11E+03	2.85E+03	2.91E+03	3.00E+03	2.86E+03	3.12E+03
	std	4.85E+00	1.28E+01	2.11E+01	9.20E+01	2.26E+01	4.37E+01	5.47E+01	2.52E+01	6.51E+01
F10	min	2.91E+03	2.91E+03	2.91E+03	2.91E+03	2.90E+03	2.90E+03	2.94E+03	2.90E+03	2.98E+03
	max	3.01E+03	3.00E+03	3.01E+03	3.01E+03	3.00E+03	3.01E+03	3.14E+03	3.00E+03	5.03E+03
	mean	2.98E+03	2.95E+03	2.94E+03	2.98E+03	2.95E+03	2.97E+03	3.04E+03	2.96E+03	3.53E+03
	std	2.57E+01	3.46E+01	3.35E+01	2.51E+01	3.21E+01	3.04E+01	4.44E+01	3.17E+01	4.74E+02

17518652, 2025, 1, Downloaded from https://ietresearch.onlinelibrary.wiley.com/doi/10.1049/cth2.70068 by Bursa Uludag University Kutuphane ve Dokumantasyon, Wiley Online Library on [07/09/2026]. See the Terms and Conditions (https://onlinelibrary.wiley.com/terms-and-conditions) on Wiley Online Library for rules of use; OA articles are governed by the applicable Creative Commons License

TABLE 3 | Wilcoxon *p*-value of the ECSA versus baseline algorithms for CEC2020.

F_No	ECSA vs CSA	ECSA vs CGO	ECSA vs HHO	ECSA vs SSA	ECSA vs GTO	ECSA vs WOA	ECSA vs PSO	ECSA vs TSA
F1	2.42E-02	5.00E-09	1.29E-06	2.88E-06	**9.71E-01**	3.02E-11	2.00E-06	4.44E-07
F2	**4.20E-01**	3.59E-05	3.96E-08	5.07E-10	7.77E-09	6.12E-10	1.11E-06	4.20E-10
F3	4.98E-11	3.02E-11	3.02E-11	4.50E-11	3.02E-11	3.02E-11	9.92E-11	3.02E-11
F4	2.53E-04	3.82E-09	3.02E-11	8.89E-10	3.02E-11	3.02E-11	1.44E-02	3.02E-11
F5	2.68E-04	3.02E-11	1.17E-05	**5.11E-01**	3.02E-11	1.73E-07	2.68E-06	2.00E-06
F6	2.67E-09	2.03E-09	3.02E-11	3.34E-11	8.89E-10	3.02E-11	3.69E-11	3.02E-11
F7	**3.71E-01**	3.02E-11	3.77E-04	**5.19E-02**	3.34E-11	1.86E-06	**1.58E-01**	6.97E-03
F8	**3.58E-01**	4.73E-04	2.75E-11	4.86E-06	1.28E-07	2.75E-11	4.92E-04	2.75E-11
F9	5.49E-11	9.92E-11	3.02E-11	4.98E-11	3.02E-11	3.02E-11	3.02E-11	3.02E-11
F10	3.67E-03	1.11E-04	**8.07E-01**	8.15E-05	**2.84E-01**	4.11E-07	4.23E-03	1.96E-10

TABLE 4 | Mean rank of Friedman's test for CEC2020.

Rankings	ECSA	CSA	CGO	HHO	SSA	GTO	WOA	PSO	TSA
Friedman's mean rank	2.5	3.4	3	6.8	4.5	4.3	7.9	4	8.6
General mean rank	1	3	2	7	6	5	8	4	9

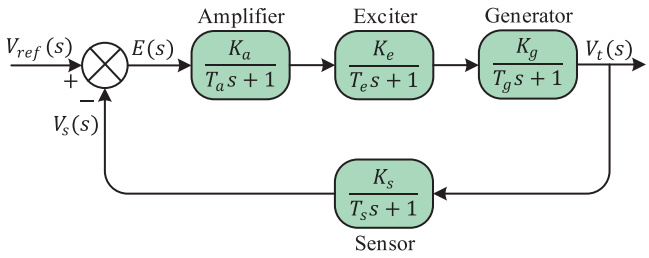


FIGURE 1 | Linearized model of AVR system.

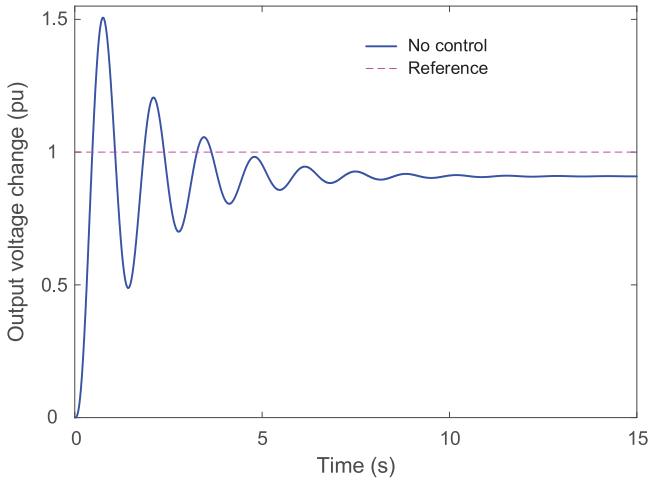


FIGURE 2 | Step response of AVR system without controller.

5 | A Novel Design Procedure via ECSA-Based Cascaded RPIDD^2-PI Controller

Numerous sectors make use of the SPID controller, as shown in Equation (1), with AVR systems being one of the most common applications [67]. In addition to the standard PID controller, AVR research has also made use of an expanded version called the SPIDD^2 controller, which is shown in Equation (4) [16].

The PIDD^2 controller increases the system's stability, steady-state error, and phase margin by adding a second-order derivative component. It should be remembered that in high-frequency domains, the derivative term in Equation (4) might not work. The potential for sensor noise to amplify control signals is a major concern that could lead to subpar system performance, so this is the case. The RPIDD^2 controller's transfer function, as shown in Equation (30) [68], can be obtained by adding a low-pass filter to the derivative component, which helps to alleviate this problem.

$$C_{RPIDD^2}(s) = K_{p1} + \frac{K_{i1}}{s} + K_{d1}\frac{N_1 s}{s+N_1} + K_{d2}\left(\frac{N_2 s}{s+N_2}\right)^2 \quad (30)$$

where K_{p1}, K_{i1}, K_{d1}, and K_{d2} denote proportional, integral, derivative, and second-order derivative gains, respectively. The filter coefficients are represented by N_1 and N_2. We have also implemented a PI controller to enhance the controller's performance. Equation (31) [69] presents the PI controller's transfer function.

$$C_{PI}(s) = K_{p2} + \frac{K_{i2}}{s} \quad (31)$$

where K_{p2} and K_{i2} are proportional and integral gains of the employed PI controller, respectively. To maximize efficacy, the adopted RPIDD^2 and PI controllers have been interconnected in

17518652, 2025, 1, Downloaded from https://ietresearch.onlinelibrary.wiley.com/doi/10.1049/cth2.70068 by Bursa Uludag University Kutuphane ve Dokumantasyon, Wiley Online Library on [07/09/2026]. See the Terms and Conditions (https://onlinelibrary.wiley.com/terms-and-conditions) on Wiley Online Library for rules of use; OA articles are governed by the applicable Creative Commons License

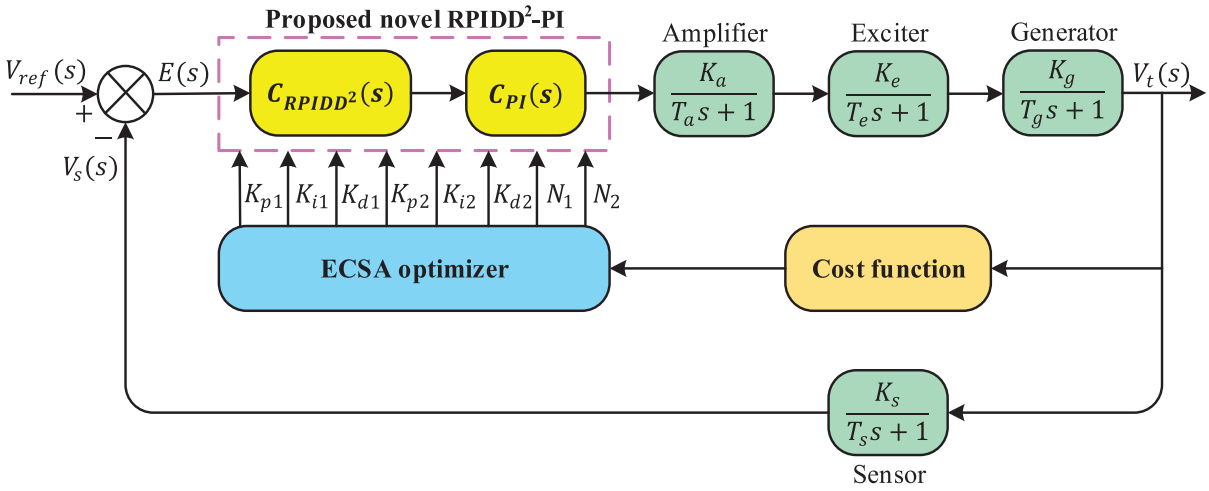


FIGURE 3 | Block diagram of ECSA-based RPIDD^2-PI controlled AVR system.

a cascaded manner which can be defined by Equation (32).

$$C_{RPIDD^2-PI}(s) = C_{RPIDD^2}(s) \times C_{PI}(s) \tag{32}$$

Using ZLG cost function, presented in Equation (5), [17] for minimization has proven to be successful in reducing the system's dynamic response performance metrics, including percentage maximum overshoot, steady-state error, settling time, and rising time.

Figure 3 shows the implementation of the ECSA optimizer to the AVR system controlled by the cascaded RPIDD^2-PI controllers. The proposed system consists of four main subsystems: the controller block, the AVR plant (amplifier, exciter, generator), the ECSA-based optimization framework, and the feedback sensor model. The control system receives the reference voltage signal $V_{ref}(s)$ and compares it with the read terminal voltage by the sensor $V_s(s)$, producing the error signal $E(s)$. This error is processed by the proposed cascaded RPIDD^2-PI controller, which consists of a reinforced proportional-integral-derivative-derivative controller handling high-order dynamic characteristics to improve transient stability and response sharpness and a conventional proportional-integral controller that complements the outer loop by stabilizing the steady-state error and ensuring smooth control effort. A core feature of the system is the ECSA optimizer, which continuously adjusts the eight controller parameters to minimize a custom-defined cost function based on time-domain error metrics. This structure ensures that both dynamic and steady-state performances are optimized. Table 5 presents the adopted parameter bounders in this study during the performing the above explained optimization procedure.

6 | Simulation Results and Validation of Proposed Approach

We have initially adopted state-of-the-art algorithms reported between 2020 and 2023 for comparisons and validation of the superior performance of the proposed control method. In this regard, cooperation search algorithm (CSA) [65], rime optimization algorithm (RIME) [70], gazelle optimization algorithm (GOA) [71], artificial rabbits optimization (ARO) [72], prairie dog optimization (PDO) [73], Runge Kutta algorithm (RUN) [74] and slime mould algorithm (SMA) [75] have been used in this study for comparative purposes.

TABLE 5 | The obtained controller parameters via ECSA.

Parameter	Lower bound	Upper bound
K_{p1}	1	4
K_{i1}	1	4
K_{d1}	1	4
K_{p2}	0.5	2
K_{i2}	0.02	1
K_{d2}	0.01	1
N_1	10	2000
N_2	10	2000

6.1 | Statistical Validation of ECSA

To comprehensively assess the performance of the ECSA in the context of AVR optimization, we conducted a thorough statistical analysis, comparing ECSA with several state-of-the-art optimization algorithms, including CSA, RIME, GOA, ARO, PDO, RUN, and SMA. For the assessment, each algorithm was subjected to 30 independent runs, each comprising 50 iterations with a fixed population size of 40 individuals. To provide a comprehensive assessment of algorithm performance, we considered several key statistical metrics. Table 6 presents the statistical performance metrics of the compared algorithms, including minimum, maximum, average, and standard deviation values. Besides, it provides the average computation time per run (elapsed times) of the algorithms. These metrics provide a quantitative measure of each algorithm's optimization performance, allowing for a precise comparison.

17518652, 2025, 1, Downloaded from https://ietresearch.onlinelibrary.wiley.com/doi/10.1049/cth2.70068 by Bursa Uludag University Kutuphane ve Dokumantasyon, Wiley Online Library on [07/09/2026]. See the Terms and Conditions (https://onlinelibrary.wiley.com/terms-and-conditions) on Wiley Online Library for rules of use; OA articles are governed by the applicable Creative Commons License

TABLE 6 | Statistical performance of compared algorithms.

Optimizer	Minimum	Maximum	Average	Standard deviation	Elapsed time (s)
ECSA	5.8086E−03	6.1089E−03	5.9394E−03	7.9591E−05	56.1621
CSA	6.4992E−03	6.9951E−03	6.6577E−03	1.2344E−04	53.3429
RIME	8.3193E−03	8.7669E−03	8.4741E−03	1.1521E−04	60.6844
GOA	6.7963E−03	7.1619E−03	6.9334E−03	9.7862E−05	55.3632
ARO	7.4505E−03	7.8066E−03	7.6169E−03	9.5874E−05	58.3595
PDO	6.9733E−03	7.5556E−03	7.1223E−03	1.2436E−04	63.2651
RUN	7.8589E−03	8.3407E−03	8.0014E−03	1.1912E−04	57.5569
SMA	8.8883E−03	9.3887E−03	9.0628E−03	1.3720E−04	61.6775

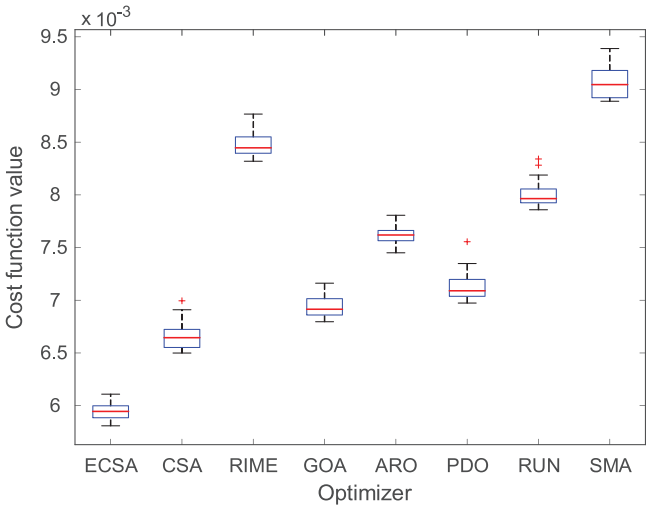


FIGURE 4 | Boxplots of ECSA, CSA, RIME, GOA, ARO, PDO, RUN and SMA optimizers.

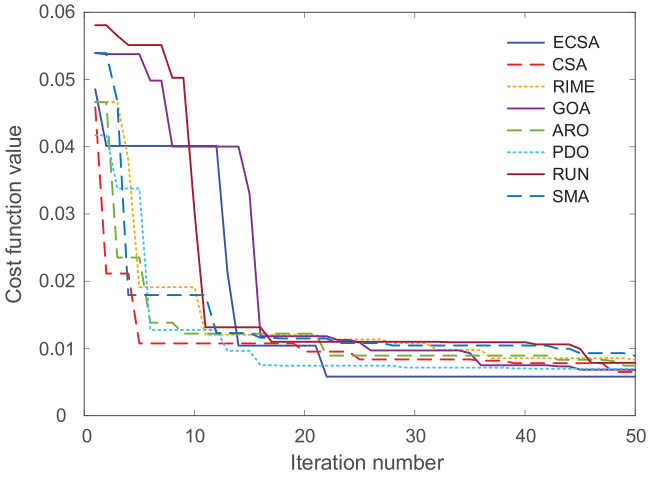


FIGURE 5 | Variation of the objective function with respect to the number of iterations.

ECSA demonstrates the lowest minimum value (5.8086E−03) among all the algorithms. This indicates that ECSA can achieve AVR system optimization with the least deviation from the desired setpoint. In practical terms, this means that ECSA is exceptionally effective at minimizing the cost function, contributing to superior voltage regulation. ECSA exhibits its superiority by having the lowest maximum value (6.1089E−03) among the algorithms. This signifies that even under challenging conditions or for the most demanding optimization scenarios, ECSA consistently maintains AVR system performance close to the desired levels. The average value for ECSA (5.9394E−03) stands out as the lowest among all the algorithms. This indicates that, on average, ECSA provides the best optimization results in terms of minimizing the cost function, leading to enhanced voltage stability and control. ECSA exhibits the smallest standard deviation (7.9591E−05) among all the algorithms. A lower standard deviation signifies that ECSA consistently delivers precise and reliable optimization results across multiple runs. This level of consistency is a crucial indicator of ECSA's robustness and reliability in AVR system control.

In Figure 4, we present boxplots visually depicting the performance distribution of ECSA and the compared algorithms. These boxplots offer insights into the central tendency, spread, and potential outliers in the optimization results. The statistical validation of ECSA, supported by both visual representations in Figure 4 and tabulated data in Table 6, offers valuable insights into its performance relative to other optimization algorithms. This analysis aids in assessing ECSA's effectiveness in optimizing AVR systems while considering key criteria such as convergence behavior, robustness, and optimization quality.

6.2 | Convergence of Cost Function

An essential aspect of evaluating the efficacy of optimization algorithms in AVR systems is examining how effectively they converge towards the desired optimization goals. In this context, we investigate the convergence behavior of the cost function, which directly reflects the quality of the AVR system's control and voltage regulation. Figure 5 provides a visual representation of how the objective function evolves concerning the number of iterations for various optimization algorithms, including the ECSA and other employed algorithms. Notably, ECSA stands out prominently in this analysis. It is evident that ECSA exhibits a remarkable convergence behavior, reaching the lowest cost function value compared to all other algorithms in the study. This signifies that ECSA swiftly and effectively navigates through the optimization landscape, fine-tuning control parameters to

17518652, 2025, 1, Downloaded from https://ietresearch.onlinelibrary.wiley.com/doi/10.1049/cth2.70068 by Bursa Uludag University Kutuphane ve Dokumantasyon, Wiley Online Library on [07/09/2026]. See the Terms and Conditions (https://onlinelibrary.wiley.com/terms-and-conditions) on Wiley Online Library for rules of use; OA articles are governed by the applicable Creative Commons License

TABLE 7 | Controller parameters obtained via other algorithms used for comparisons.

Optimizer	K_{p1}	K_{i1}	K_{d1}	K_{p2}	K_{i2}	K_{d2}	N_1	N_2
ECSA	3.8665	0.74127	1.3253	1.3444	0.28547	0.11818	1886.6	1999.9
CSA	3.1291	0.84604	1.2983	1.3565	0.40802	0.10959	639.53	1899.6
RIME	3.7913	0.81081	1.3862	1.1912	0.37978	0.11899	707.10	1994.7
GOA	3.1671	0.90594	1.5835	1.0765	0.52558	0.13450	388.63	1389.5
ARO	3.4065	0.95164	1.9097	0.89184	0.50644	0.15494	1727.3	1489.3
PDO	2.7169	0.84154	1.2185	1.3935	0.52699	0.10258	1199.6	1167.2
RUN	3.6191	1.2401	1.3141	1.2712	0.23356	0.10636	1193.4	1176.1
SMA	2.8548	1.1215	1.5188	1.0630	0.45792	0.11451	1940.1	1269.4

minimize the cost function. In the subsequent sections, we delve deeper into the performance evaluation of ECSA and its impact on AVR system dynamics, further elucidating its role in achieving superior control and voltage stability.

6.3 | Transient Stability Performance Evaluation

The transient stability of an AVR system plays a critical role in ensuring the reliable operation of electrical networks during dynamic conditions. To assess and compare the transient stability performance of different optimization algorithms, we examine key metrics such as rise time, settling time, percent overshoot, and peak time. These metrics provide valuable insights into the responsiveness and robustness of AVR control systems. In Table 7, we present the controller parameters obtained through various optimization algorithms, including ECSA and other optimization methods used for comparisons. These parameters serve as the foundation for evaluating the transient stability of the AVR system under consideration.

Using the controller parameters from Table 7 and the block diagram in Figure 3, we derive the transfer functions for ECSA and the compared algorithms. The closed-loop transfer functions for ECSA and each algorithm are presented in Equations (33)–(40), representing their respective control configurations. Equations (33)–(40) demonstrate the mathematical representations of the AVR system's transfer functions, highlighting the intricate relationships between the controller parameters and the system's response to varying inputs.

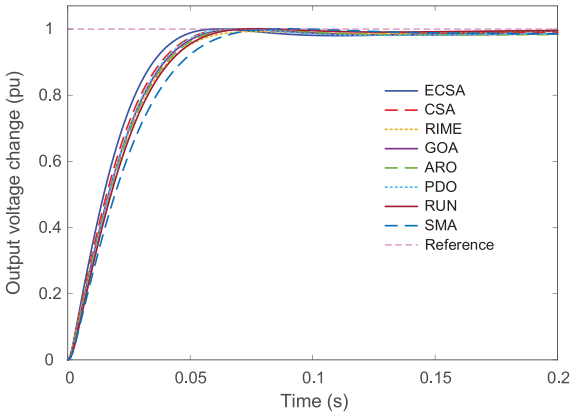


FIGURE 6 | Step responses of controlled AVR system optimized by recent algorithms.

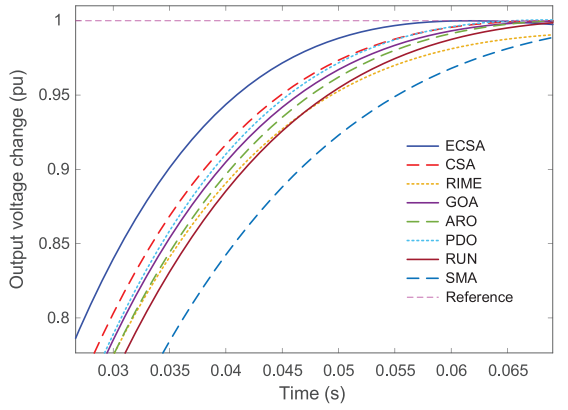


FIGURE 7 | Zoomed view of step responses of controlled AVR system optimized by recent algorithms.

$$T_{ECSA}(s) = \frac{6.388e04s^6 + 1.276e08s^5 + 1.35e10s^4 + 1.418e11s^3 + 4.226e11s^2 + 1.587e11s + 1.597e10}{0.0004s^9 + 2.4s^8 + 4886s^7 + 3.546e06s^6 + 3.554e08s^5 + 1.633e10s^4 + 1.49e11s^3 + 4.286e11s^2 + 1.585e11s + 1.597e10} \quad (33)$$

$$T_{CSA}(s) = \frac{5.376e04s^6 + 4.013e07s^5 + 3.895e09s^4 + 4.305e10s^3 + 1.109e11s^2 + 5.605e10s + 7.966e09}{0.0004s^9 + 1.821s^8 + 2617s^7 + 1.2e06s^6 + 1.135e08s^5 + 4.765e09s^4 + 4.543e10s^3 + 1.126e11s^2 + 5.597e10s + 7.966e09} \quad (34)$$

$$T_{RIME}(s) = \frac{5.651e04s^6 + 4.602e07s^5 + 4.517e09s^4 + 4.947e10s^3 + 1.427e11s^2 + 6.779e10s + 8.663e09}{0.0004s^9 + 1.924s^8 + 2934s^7 + 1.437e06s^6 + 1.372e08s^5 + 5.608e09s^4 + 5.231e10s^3 + 1.448e11s^2 + 6.77e10s + 8.663e09} \quad (35)$$

$$T_{GOA}(s) = \frac{2.802e04s^6 + 1.386e07s^5 + 1.241e09s^4 + 1.375e10s^3 + 3.21e10s^2 + 1.986e10s + 3.573e09}{0.0004s^9 + 1.312s^8 + 1349s^7 + 4.386e05s^6 + 3.854e07s^5 + 1.527e09s^4 + 1.457e10s^3 + 3.266e10s^2 + 1.982e10s + 3.573e09} \quad (36)$$

17518652, 2025, 1, Downloaded from https://ietresearch.onlinelibrary.wiley.com/doi/10.1049/cth2.70068 by Bursa Uludag University Kutuphane ve Dokumantasyon, Wiley Online Library on [07/09/2026]. See the Terms and Conditions (https://onlinelibrary.wiley.com/terms-and-conditions) on Wiley Online Library for rules of use; OA articles are governed by the applicable Creative Commons License

$$T_{ARO}(s) = \frac{3.094e04s^6 + 5.693e07s^5 + 6.069e09s^4 + 7.007e10s^3 + 1.546e11s^2 + 9.883e10s + 1.846e10}{0.0004s^9 + 1.928s^8 + 3159s^7 + 1.869e06s^6 + 1.811e08s^5 + 7.521e09s^4 + 7.432e10s^3 + 1.575e11s^2 + 9.865e10s + 1.846e10} \quad (37)$$

$$T_{PDO}(s) = \frac{1.968e04s^6 + 2.581e07s^5 + 2.673e09s^4 + 2.953e10s^3 + 7.29e10s^2 + 4.266e10s + 7.248e09}{0.0004s^9 + 1.459s^8 + 1826s^7 + 8.447e05s^6 + 7.848e07s^5 + 3.298e09s^4 + 3.128e10s^3 + 7.411e10s^2 + 4.258e10s + 7.248e09} \quad (38)$$

$$T_{RUN}(s) = \frac{1.89e04s^6 + 2.468e07s^5 + 2.561e09s^4 + 2.9e10s^3 + 8.151e10s^2 + 4.004e10s + 4.781e09}{0.0004s^9 + 1.464s^8 + 1838s^7 + 8.525e05s^6 + 7.916e07s^5 + 3.202e09s^4 + 3.068e10s^3 + 8.276e10s^2 + 3.999e10s + 4.781e09} \quad (39)$$

$$T_{SMA}(s) = \frac{1.993e04s^6 + 4.085e07s^5 + 4.409e09s^4 + 5.351e10s^3 + 1.176e11s^2 + 7.833e10s + 1.605e10}{0.0004s^9 + 1.837s^8 + 2819s^7 + 1.55e06s^6 + 1.476e08s^5 + 5.631e09s^4 + 5.707e10s^3 + 1.199e11s^2 + 7.817e10s + 1.605e10} \quad (40)$$

Figures 6–11 depict visual comparisons of critical transient stability metrics for AVR systems optimized by recent algorithms. These figures provide insights into how each algorithm influences the system's response during dynamic events. Notably, ECSA stands out prominently in these visual comparisons, showcasing its exceptional performance in key aspects of transient stability. Specifically, ECSA achieves a minimum rise time of 0.0314 s, indicating its ability to rapidly respond to changes in system conditions. It also demonstrates a minimum settling time of 0.0472 s, signifying its capacity to reach a stable state swiftly. ECSA, along with CSA and GOA, achieves zero percent overshoot, indicating precise control and minimal oscillations. The

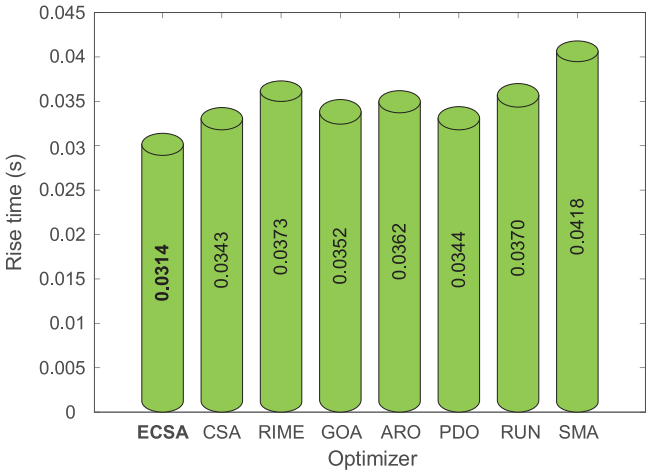


FIGURE 8 | Visual comparison of rise times.

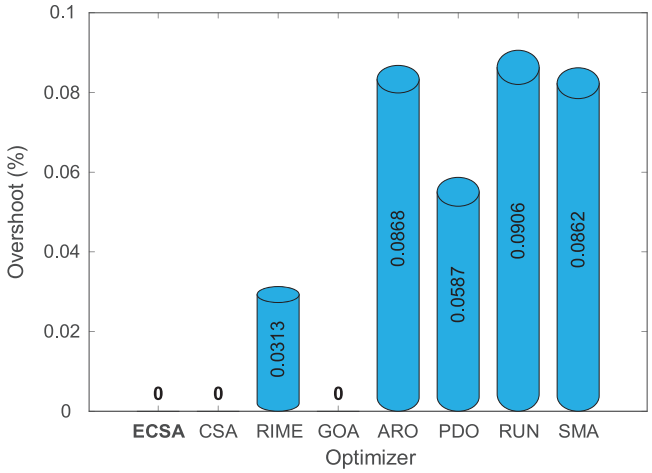


FIGURE 10 | Visual comparison of percent overshoots.

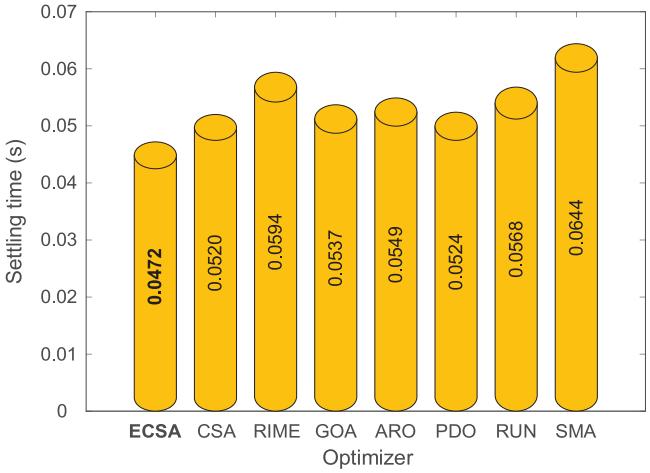


FIGURE 9 | Visual comparison of settling times.

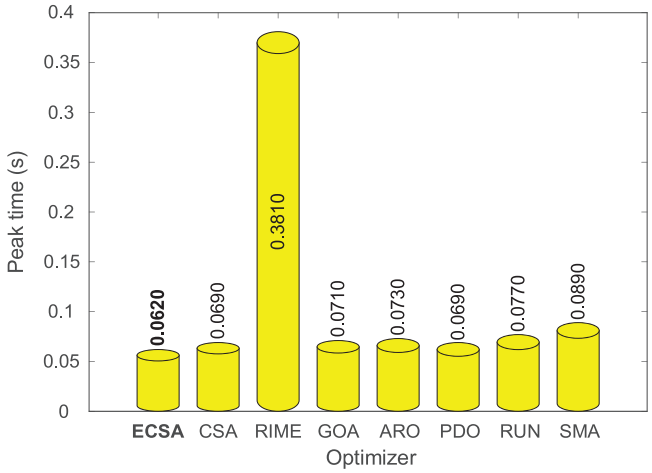


FIGURE 11 | Visual comparison of peak times.

17518652, 2025, 1, Downloaded from https://ietresearch.onlinelibrary.wiley.com/doi/10.1049/cth2.70068 by Bursa Uludag University Kutuphane ve Dokumantasyon, Wiley Online Library on [07/09/2026]. See the Terms and Conditions (https://onlinelibrary.wiley.com/terms-and-conditions) on Wiley Online Library for rules of use; OA articles are governed by the applicable Creative Commons License

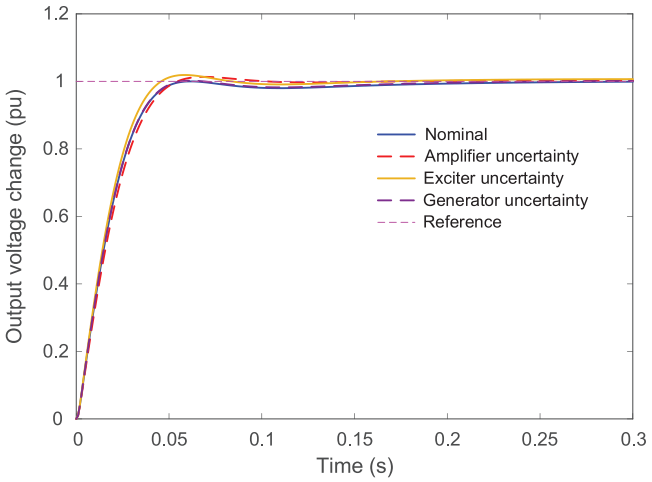


FIGURE 12 | Step response of the cascaded RPIDD^2-PI controller tuned with ECSA.

proposed ECSA further exhibits a minimum peak time of 0.0620 s, showcasing its efficiency in reaching peak system responses. These results underscore ECSA's superiority in enhancing the transient stability of AVR systems, ensuring rapid response to disturbances, minimal oscillations, and swift recovery to steady-state conditions. ECSA's outstanding performance in these critical metrics positions it as a highly effective optimization algorithm for AVR control and voltage regulation. In the Appendix section, MATLAB codes are provided for the ECSA-optimized RPIDD^2-PI controller-based AVR system, enabling readers to validate and further explore ECSA's impact on transient stability.

6.4 | Robustness Analysis

Robustness analysis is a crucial aspect of evaluating the effectiveness and reliability of control systems, especially in the context of AVR systems where uncertainties in system components can have a significant impact on performance. In this section, we examine the robustness of the cascaded RPIDD^2-PI controller tuned with the ECSA concerning uncertainties in key system components, including amplifiers, exciters, and generators. To assess the robustness of the controller, we introduce uncertainties in the following system parameters.

Amplifier uncertainty: $K_a = 10.75$ and $T_a = 0.115$ s
Exciter uncertainty: $K_e = 1.3$ and $T_e = 0.5$ s
Generator uncertainty: $K_g = 1.1$ and $T_g = 1.1$ s

Figure 12 presents the step response of the cascaded RPIDD^2-PI controller when tuned with ECSA. This response illustrates how the system behaves in the presence of uncertainties and provides insights into its transient stability.

Table 8 provides a comprehensive overview of the transient response performance of the ECSA-based RPIDD^2-PI controller under various uncertainty scenarios. The performance metrics include rise time, settling time, overshoot, and peak time. Comparing the performance metrics of the nominal case with those under different uncertainty scenarios, we observe minimal deviations. The maximum deviations from nominal values are as follows: 0.0025 s for rise time, 0.058 s for settling time, 1.8976% for overshoot, and 0.0070 s for peak time. These deviations are remarkably small, confirming that the proposed control approach is highly robust to parameter variations. In the context of an AVR system, these results indicate that the controller can maintain stable and reliable voltage regulation even in the presence of uncertainties in amplifier, exciter, and generator parameters. The robustness analysis results provide confidence in the resilience of the ECSA-tuned cascaded RPIDD^2-PI controller, emphasizing its ability to effectively mitigate the effects of parameter variations and ensure consistent AVR system performance.

6.5 | Comparisons of Time Response Quality Metrics with Reported Metaheuristic-Based Various Controller Types

In this section, we conduct a comprehensive analysis to assess the performance of the proposed ECSA-based RPIDD^2-PI controller in comparison to various other controller types reported in the literature. The aim is to showcase the efficacy of our proposed approach by comparing its time response quality metrics with those of 44 different controller approaches discussed in 29 published papers. Specifically, we focus on contemporary and efficient methods reported in recent years for a thorough evaluation. Table 9 provides a detailed comparative analysis of time response quality metrics for different controller approaches. The metrics evaluated include rise time, settling time, overshoot, and peak time.

Among the considered controller types, various approaches exhibit diverse performance characteristics. Some approaches achieve excellent performance in certain metrics but may have limitations in others. Notably, the ECSA-based RPIDD^2-PI controller demonstrates impressive performance metrics (rise time: 0.0314 s, settling time: 0.0472 s, overshoot: 0%, peak time: 0.062 s. To put the performance of the ECSA-based RPIDD^2-PI controller into perspective, we highlight a few notable comparisons. When compared to SPID controllers, the ECSA-based approach exhibits significantly improved metrics. For example, it achieves a remarkable reduction in overshoot, which is crucial for maintaining system stability. In the realm of FOPID controllers, the ECSA-tuned RPIDD^2-PI controller surpasses other FOPID-based controllers by achieving a lower rise time and settling time, indicating superior dynamic response. Compared to other recent metaheuristic-based controllers, the ECSA-based approach consistently delivers competitive or superior performance across all metrics, showcasing its effectiveness in AVR system control. Overall, the comparative analysis underscores the robustness and superior time response characteristics of the ECSA-based RPIDD^2-PI controller, further validating its potential as an advanced and efficient solution for AVR systems.

6.6 | Discussion

The optimization of AVR systems is a critical aspect of ensuring the reliable operation of electrical networks. In this study, we have explored the effectiveness of the ECSA in tuning the

17518652, 2025, 1, Downloaded from https://ietresearch.onlinelibrary.wiley.com/doi/10.1049/cth2.70068 by Bursa Uludag University Kutuphane ve Dokumantasyon, Wiley Online Library on [07/09/2026]. See the Terms and Conditions (https://onlinelibrary.wiley.com/terms-and-conditions) on Wiley Online Library for rules of use; OA articles are governed by the applicable Creative Commons License

TABLE 8 | Transient response performance of the ECSA-based RPIDD^2-PI controller with respect to amplifier, exciter and generator uncertainties.

Case	Rise time (s)	Settling time (s)	Overshoot (%)	Peak time (s)
Nominal	0.0314	0.0472	0	0.0620
Amplifier uncertainty	0.0331	0.0483	1.3438	0.0690
Exciter uncertainty	0.0289	0.0414	1.8976	0.0580
Generator uncertainty	0.0313	0.0467	0.2180	0.0620

cascaded RPIDD^2-PI controller for AVR systems. Our investigation involved a thorough analysis of ECSA's performance in comparison to several state-of-the-art optimization algorithms reported between 2020 and 2023. Statistical validation was a fundamental aspect of this study, aiming to assess ECSA's performance comprehensively. ECSA demonstrated superior optimization performance across various statistical metrics when compared to other algorithms, including CSA, RIME, GOA, ARO, PDO, RUN, and SMA. Notably, ECSA exhibited the lowest minimum value, signifying its ability to achieve AVR system optimization with minimal deviation from the desired setpoint. Furthermore, ECSA consistently maintained AVR system performance close to desired levels, even under challenging conditions or demanding scenarios, as indicated by its lowest maximum value. The average value for ECSA was also the lowest among all the algorithms, highlighting its ability to provide the best optimization results in terms of minimizing the cost function. Additionally, ECSA demonstrated the smallest standard deviation, signifying its reliability and robustness in delivering precise and consistent optimization results across multiple runs. This robustness is a crucial indicator of ECSA's suitability for AVR system control, where reliability and stability are paramount. Another essential aspect of evaluating optimization algorithms for AVR systems is their convergence behavior. ECSA showcased remarkable convergence behavior, consistently achieving the lowest cost function value compared to other algorithms. This effective convergence indicates ECSA's ability to fine-tune control parameters efficiently, contributing to the minimization of the cost function. This, in turn, results in enhanced voltage regulation and control within the AVR system. Transient stability is also a critical consideration for AVR systems, particularly during dynamic conditions. ECSA excelled in this aspect, achieving minimal rise time, settling time, percent overshoot, and peak time. These metrics collectively indicate ECSA's capacity to respond swiftly to changes in system conditions, minimize oscillations, and quickly return the system to a stable state. ECSA's exceptional performance in transient stability metrics positions it as an effective optimization algorithm for AVR control and voltage regulation, especially in scenarios where rapid responses are crucial. Robustness analysis is vital, especially in real-world applications where uncertainties in system components can impact performance. ECSA-tuned controllers were evaluated under uncertainties in amplifier, exciter, and generator parameters. The results demonstrated that the ECSA-based controller maintained stable voltage regulation, even in the presence of parameter variations. The deviations from nominal values were remarkably small, underscoring the controller's robustness and resilience to uncertainties.

To contextualize the performance of the ECSA-based RPIDD^2-PI controller, we conducted a comparative analysis with various other controller types reported in the literature. ECSA consistently outperformed other controller types across critical metrics, including rise time, settling time, overshoot, and peak time. Notably, ECSA's reduction in overshoot is crucial for maintaining system stability. These results are quantitatively demonstrated in Tables 8 and 9, which presents a comprehensive time-domain performance comparison. It can be clearly seen that the ECSA-tuned RPIDD^2-PI controller achieves the lowest rise time and settling time while completely eliminating overshoot, confirming its superiority over the benchmark methods. In comparison to other controllers, ECSA achieved lower rise and settling times, indicating superior dynamic response. The results of this study have significant implications for the optimization of AVR systems in power networks. ECSA has proven to be an effective algorithm for fine-tuning control parameters, leading to enhanced voltage regulation, transient stability, and robust performance. In conclusion, the study demonstrates that ECSA-based optimization is a promising approach for enhancing AVR system performance. Its effectiveness in minimizing cost functions, rapid convergence, robustness to uncertainties, and superior transient stability position it as a valuable tool for ensuring reliable and stable electrical networks.

7 | Conclusion

In this study, we introduced a groundbreaking solution for enhancing the precision, stability, and responsiveness of AVR systems. Our novel approach introduces a cascaded RPIDD^2-PI controller specifically designed to address the limitations associated with conventional control methods. This controller scheme is proposed for the first time in literature. To further elevate its efficacy, we integrated an enhanced cooperation search algorithm (ECSA), incorporating control randomization, linear transfer functions, new exploration and exploitation stages, and a greedy selection strategy. The integration of ECSA marked a significant leap in optimizing AVR systems, as evidenced by our comprehensive comparative analysis against state-of-the-art optimization algorithms reported between 2020 and 2023. Our findings unveil ECSA's exceptional performance in optimizing AVR systems, consistently surpassing its counterparts across key statistical metrics. The ability to achieve minimal deviation from setpoints, even under challenging scenarios, establishes ECSA's contribution to heightened voltage stability. Moreover, its unwavering precision and reliability, as demonstrated by low standard deviation values across multiple runs, reinforce

17518652, 2025, 1, Downloaded from https://ietresearch.onlinelibrary.wiley.com/doi/10.1049/cth2.70068 by Bursa Uludag University Kutuphane ve Dokumantasyon, Wiley Online Library on [07/09/2026]. See the Terms and Conditions (https://onlinelibrary.wiley.com/terms-and-conditions) on Wiley Online Library for rules of use; OA articles are governed by the applicable Creative Commons License

TABLE 9 | Comparative time response quality metrics analysis with respect to other reported metaheuristic-based different controller types.

Ref.	Approach	Rise time (s)	Settling time (s)	Overshoot (%)	Peak time (s)
[18]	SCA-based SPID	0.148	0.724	11.4	0.304
[19]	TSA-based SPID	0.131	0.758	15.57	0.278
[20]	L-RSANM-based SPID	0.3076	0.4669	0.9582	0.6023
[21]	EWOA-based SPID	0.2308	1.0420	17.20	0.3260
[9]	ChBWO-based FOPID	0.1103	0.169	1.1838	Not reported
[22]	IGBO-based FOPID	0.0899	0.932	8.36	0.176
[23]	MGWO-based FOPID	0.0427	0.0653	**0**	Not reported
[24]	MSFA-based FOPID	0.1415	0.1922	0.3628	Not reported
[25]	SA-MRFO-based SPID	0.2540	0.3802	1.7999	Not reported
	SA-MRFO-based RPID	0.2576	0.3871	1.7283	Not reported
	SA-MRFO-based FOPID	0.1309	0.1909	1.9765	Not reported
	SA-MRFO-based SPIDD^2	0.0535	0.0798	0.7562	Not reported
[26]	SOS-based RPID	0.267	0.371	0.007	Not reported
[7]	AOA-based SPID	0.2510	0.3746	1.9393	Not reported
	AOA-based RPID	0.2549	0.3816	1.9977	Not reported
	AOA-based FOPID	0.1040	0.1480	1.3234	Not reported
	AOA-based SPIDD^2	0.0531	0.0800	0.4996	Not reported
[27]	L-RUN-based SPIDD^2	0.0357	0.0537	**0**	0.0725
[28]	enAO-based SPIDD^2	0.0357	0.0535	**0**	0.0726
[29]	FDB-LFD-based SPID	0.263	0.362	1.51	Not reported
	FDB-LFD-based RPID	0.266	0.368	1.48	Not reported
	FDB-LFD-based FOPID	0.140	0.187	2.53	Not reported
	FDB-LFD-based SPIDD^2	0.063	0.081	1.70	Not reported
[30]	EO-based TI$^\lambda$DND^{2}N^2	0.03752	0.0596	0.4128	Not reported
[31]	GA-based resilient PID	Not reported	0.4792	1.9756	Not reported
[32]	Rao-based MFOPID	0.0965	0.170	0.01	0.317
[33]	SCA-based FOPIDFF	0.1230	0.1670	0.1262	Not reported
[34]	PSO-based 2DOF PI	0.690	3.442	2.224	3.296
[35]	PSO-based FHODFC	0.373	0.685	0.001	0.815
	PSO-based HODFC	0.571	0.989	1.150	1.401
[36]	NSCA-based sigmoid PID	0.498	0.579	2.2	Not reported
[37]	GA-based fuzzy PID	0.1857	0.2963	1.0407	Not reported
[38]	ICA-based gray PID	0.2305	0.3193	1.23	Not reported
[39]	EO-based FOPID-DN	0.076	0.144	**0**	0.837
[40]	COA-based FOPID	0.1011	0.1474	1.952	Not reported
	COA-based PI$^\lambda$DND^{2}N^2	0.0400	0.0617	1.596	Not reported
[41]	ICA-based NN predictive	Not reported	1.9067	0.6	Not reported

(Continues)

17518652, 2025, 1, Downloaded from https://ietresearch.onlinelibrary.wiley.com/doi/10.1049/cth2.70068 by Bursa Uludag University Kutuphane ve Dokumantasyon, Wiley Online Library on [07/09/2026]. See the Terms and Conditions (https://onlinelibrary.wiley.com/terms-and-conditions) on Wiley Online Library for rules of use; OA articles are governed by the applicable Creative Commons License

TABLE 9 | (Continued)

Ref.	Approach	Rise time (s)	Settling time (s)	Overshoot (%)	Peak time (s)
[11]	RSA-based SPID	0.3006	0.4563	0.9179	0.5787
	RSA-based FOPID	0.1499	0.2201	1.2933	0.8757
	RSA-based SPIDD^2	0.0674	0.1245	0.0060	0.5961
	RSA-based FOPIDD^2	0.0487	0.0806	**0**	0.1287
[42]	WOA-based SPID	0.26	0.555	7	Not reported
	WOA-based PIDA	0.328	0.453	2	Not reported
[43]	iRUN-based RPIDD^2	0.0399	0.0626	**0**	Not reported
This study	ECSA-based RPIDD^2-PI	**0.0314**	**0.0472**	**0**	**0.0620**

its robustness in AVR system control. In terms of convergence behavior, ECSA exhibited remarkable swiftness in fine-tuning control parameters, minimizing the cost function effectively. The optimization results were not limited to numerical excellence but also translated into tangible benefits for transient stability. The cascaded RPIDD^2-PI controller tuned via ECSA demonstrated reduced rise time, settling time, percent overshoot, and peak time, ensuring rapid responses to dynamic conditions and minimal oscillations. Additionally, our robustness analysis underscored proposed method's resilience to uncertainties in system components, guaranteeing stable voltage regulation under variable conditions. Comparative assessments against other controller types reported in the literature consistently positioned our proposed method as an advanced and efficient solution for AVR systems, offering superior performance across key metrics. While our study has achieved significant milestones, several promising avenues for future research emerge. Investigating the potential of hybrid algorithms that combine ECSA with other optimization techniques could yield further performance enhancements in AVR system control. Applying the ECSA-tuned control mechanism in real-world power systems to assess its practical viability and scalability is a crucial next step. Incorporating machine learning techniques to adaptively optimize AVR systems based on changing network conditions and demands is a promising direction.

Author Contributions

Davut Izci, **Fatma A. Hashim**, **Serdar Ekinci:** conceptualization, methodology, software, visualization, investigation, writing – original draft preparation. **Sahar F. Sabbeh:** data curation, validation, supervision, resources, writing – review & editing. **Mohit Bajaj**, **Lukas Prokop**, **Ievgen Zaitsev:** project administration, supervision, resources, writing – review & editing.

Acknowledgements

This research is funded by European Union under the REFRESH—Research Excellence For Region Sustainability and High-Tech Industries Project via the Operational Programme Just Transition under Grant CZ.10.03.01/00/22_003/0000048; in part by the National Centre for Energy II and ExPEDite Project a Research and Innovation Action to Support the Implementation of the Climate Neutral and Smart Cities Mission Project TN02000025; and in part by ExPEDite through European Union's Horizon Mission Programme under Grant 101139527. The authors would like to express their sincere gratitude to Stanislav Misak for his exceptional supervision, project administration, and overall guidance throughout the course of this project. His expertise and support were instrumental to its success.

Conflicts of Interest

On behalf of all authors, the corresponding author states that there are no conflicts of interest.

Data Availability Statement

The datasets used and/or analysed during the current study are available from the corresponding author on reasonable request.

References

1. O. Can, S. Ekinci, and D. Izci, "Honey Badger Algorithm for Adjustment of FOPID Controller Adopted in an Automatic Voltage Regulator System", in *2022 Global Energy Conference (GEC)* (IEEE, 2022), 262–265.

2. S. Duman, N. Yörükeren, and İ. H. Altaş, "Gravitational Search Algorithm for Determining Controller Parameters in an Automatic Voltage Regulator System," *Turkish Journal of Electrical Engineering & Computer Sciences* 24, no. 4 (2016): 2387–2400.

3. S. Ekinci, V. Snášel, R. M. Rizk-Allah, D. Izci, M. Salman, and A. A. F. Youssef, "Optimizing AVR System Performance via a Novel Cascaded RPIDD2-FOPI Controller and QWGBO Approach," *PLoS ONE* 19, no. 5 (2024): e0299009.

4. D. Izci, L. Abualigah, Ö. Can, C. Andiç, and S. Ekinci, "Achieving Improved Stability for Automatic Voltage Regulation With Fractional-order PID plus Double-derivative Controller and Mountain Gazelle Optimizer," *International Journal of Dynamics and Control* 12, no. 7 (2024): 2550–2565.

5. S. Ekinci, Ö. Can, and D. Izci, "Controller Design for Automatic Voltage Regulator System Using Modified Opposition-based Weighted Mean of Vectors Algorithm," *International Journal of Modelling and Simulation* 45, no. 4 (2023): 1–18.

6. E. Celik, "Incorporation of Stochastic Fractal Search Algorithm Into Efficient Design of PID Controller for an Automatic Voltage Regulator System," *Neural Computing and Applications* 30, no. 6 (2018): 1991–2002.

7. A. Agwa, S. Elsayed, and M. Ahmed, "Design of Optimal Controllers for Automatic Voltage Regulation Using Archimedes Optimizer," *Intelligent Automation & Soft Computing* 31, no. 2 (2022): 799–815.

8. A. M. Mosaad, M. A. Attia, and A. Y. Abdelaziz, "Comparative Performance Analysis of AVR Controllers Using Modern Optimization

17518652, 2025, 1, Downloaded from https://ietresearch.onlinelibrary.wiley.com/doi/10.1049/cth2.70068 by Bursa Uludag University Kutuphane ve Dokumantasyon, Wiley Online Library on [07/09/2026]. See the Terms and Conditions (https://onlinelibrary.wiley.com/terms-and-conditions) on Wiley Online Library for rules of use; OA articles are governed by the applicable Creative Commons License

Techniques," *Electric Power Components and Systems* 46, no. 19–20 (2018): 2117–2130.

9. V. K. Munagala and R. K. Jatoth, "Improved Fractional PIλDμ Controller for AVR System Using Chaotic Black Widow Algorithm," *Computers & Electrical Engineering* 97 (2022): 107600.

10. D. Mokeddem and S. Mirjalili, "Improved Whale Optimization Algorithm Applied to Design PID Plus Second-Order Derivative Controller for Automatic Voltage Regulator System," *Journal of the Chinese Institute of Engineers* 43, no. 6 (2020): 541–552.

11. Ö. Can, C. Andiç, S. Ekinci, and D. Izci, "Enhancing Transient Response Performance of Automatic Voltage Regulator System by Using a Novel Control Design Strategy," *Electrical Engineering* 105, no. 4 (2023): 1993–2005.

12. D. Izci, "Design and Application of an Optimally Tuned PID Controller for DC Motor Speed Regulation via a Novel Hybrid Lévy Flight Distribution and Nelder–Mead Algorithm," *Transactions of the Institute of Measurement and Control* 43, no. 14 (2021): 3195–3211.

13. N. I. Smirnov, V. R. Sabanin, and A. I. Repin, "Sensitivity and Robust Tuning of PID Controllers With Real Differentiation," *Thermal Engineering* 54, no. 10 (2007): 777–785.

14. H. Sarma and A. Bardalai, "Improvisation of Artificial Hummingbird Algorithm Through Incorporation of Chaos Theory in Intelligent Optimization of Fractional Order PID Controller Tuning," *International Journal of Information Technology* (2024).

15. H. Abdelfattah, A. O. Aseeri, and M. Abd Elaziz, "Optimized FOPID Controller for Nuclear Research Reactor Using Enhanced Planet Optimization Algorithm," *Alexandria Engineering Journal* 97 (2024): 267–282.

16. D. Izci, S. Ekinci, and H. L. Zeynelgil, "Controlling an Automatic Voltage Regulator Using a Novel Harris hawks and Simulated Annealing Optimization Technique," *Advanced Control for Applications* 6, no. 2 (2024): e121.

17. Y. Danayiyen, K. Dinçer, and Y. Nuhoğlu, "A Novel Fractional Order Proportional Integral-Fractional Order Proportional Derivative Controller Design Based on Symbiotic Organisms Search Algorithm for Speed Control of a Direct Current Motor," *Electrica* 24, no. 2 (2024): 327–335.

18. B. Hekimoğlu, "Sine-Cosine Algorithm-Based Optimization for Automatic Voltage Regulator System," *Transactions of the Institute of Measurement and Control* 41, no. 6 (2019): 1761–1771.

19. E. Kose, "Optimal Control of AVR System with Tree Seed Algorithm-Based PID Controller," *IEEE Access* 8 (2020): 89457–89467.

20. S. Ekinci, D. Izci, R. Abu Zitar, A. R. Alsoud, and L. Abualigah, "Development of Lévy Flight-based Reptile Search Algorithm With Local Search Ability for Power Systems Engineering Design Problems," *Neural Computing and Applications* 34, no. 22 (2022): 20263–20283.

21. J. Zhang, T. Zhang, G. Zhang, and M. Kong, "Parameter Optimization of PID Controller Based on an Enhanced Whale Optimization Algorithm for AVR System," *Operational Research* 23, no. 3 (2023): 44.

22. S. M. A. Altbawi, S. B. A. Khalid, et al., "An Improved Gradient-Based Optimization Algorithm for Solving Complex Optimization Problems," *Processes* 11, no. 2 (2023): 498.

23. S. K. Verma and R. Devarapalli, "Fractional Order PIλDμ Controller With Optimal Parameters Using Modified Grey Wolf Optimizer for AVR System" *Archives of Control Sciences* 32, no. 2 (2023): 429–450.

24. R. Mok and M. A. Ahmad, "Fast and Optimal Tuning of Fractional Order PID Controller for AVR System Based on Memorizable-smoothed Functional Algorithm," *Engineering Science and Technology, an International Journal* 35 (2022): 101264.

25. M. Micev, M. Ćalasan, Z. M. Ali, H. M. Hasanien, and S. H. E. Abdel Aleem, "Optimal Design of Automatic Voltage Regulation Controller Using Hybrid Simulated Annealing—Manta Ray Foraging Optimization Algorithm," *Ain Shams Engineering Journal* 12, no. 1 (2021): 641–657.

26. B. Ozgenc, M. S. Ayas, and I. H. Altas, "Performance Improvement of an AVR System by Symbiotic Organism Search Algorithm-based PID-F Controller," *Neural Computing and Applications* 34, no. 10 (2022): 7899–7908.

27. D. Izci, S. Ekinci, S. Mirjalili, and L. Abualigah, "An Intelligent Tuning Scheme With a Master/Slave Approach for Efficient Control of the Automatic Voltage Regulator," *Neural Computing and Applications* 35, no. 26 (2023): 19099–19115.

28. S. Ekinci, D. Izci, E. Eker, and L. Abualigah, "An Effective Control Design Approach Based on Novel Enhanced aquila Optimizer for Automatic Voltage Regulator," *Artificial Intelligence Review* 56, no. 2 (2023): 1731–1762.

29. H. Bakir, U. Guvenc, H. Tolga Kahraman, and S. Duman, "Improved Lévy Flight Distribution Algorithm With FDB-based Guiding Mechanism for AVR System Optimal Design," *Computers & Industrial Engineering* 168 (2022): 108032.

30. A. Tabak, "Novel TIλDND2N2 Controller Application With Equilibrium Optimizer for Automatic Voltage Regulator," *Sustainability* 15, no. 15 (2023): 11640.

31. M. Elsisi, "Optimal Design of Non-fragile PID Controller," *Asian Journal of Control* 23, no. 2 (2021): 729–738.

32. N. Paliwal, L. Srivastava, and M. Pandit, "Rao Algorithm Based Optimal Multi-term FOPID Controller for Automatic Voltage Regulator System," *Optimal Control Applications and Methods* 43, no. 6 (2022): 1707–1734.

33. M. S. Ayas and E. Sahin, "FOPID Controller With Fractional Filter for an Automatic Voltage Regulator," *Computers & Electrical Engineering* 90 (2021): 106895.

34. H. Gozde, "Robust 2DOF state-feedback PI-controller Based on Metaheuristic Optimization for Automatic Voltage Regulation System," *ISA Transactions* 98 (2020): 26–36.

35. M. S. Ayas, "Design of an Optimized Fractional High-order Differential Feedback Controller for an AVR System," *Electrical Engineering* 101, no. 4 (2019): 1221–1233.

36. M. H. Suid and M. A. Ahmad, "Optimal Tuning of Sigmoid PID Controller Using Nonlinear Sine Cosine Algorithm for the Automatic Voltage Regulator System," *ISA Transactions* 128 (2022): 265–286.

37. T. Dogruer and M. S. Can, "Design and Robustness Analysis of Fuzzy PID Controller for Automatic Voltage Regulator System Using Genetic Algorithm," *Transactions of the Institute of Measurement and Control* 44, no. 9 (2022): 1862–1873.

38. Y. Tang, L. Zhao, Z. Han, X. Bi, and X. Guan, "Optimal Gray PID Controller Design for Automatic Voltage Regulator System via Imperialist Competitive Algorithm," *International Journal of Machine Learning and Cybernetics* 7, no. 2 (2016): 229–240.

39. N. Paliwal, L. Srivastava, and M. Pandit, "Equilibrium Optimizer Tuned Novel FOPID-DN Controller for Automatic Voltage Regulator System," *International Transactions on Electrical Energy Systems* 31, no. 8 (2021).

40. I. Moschos and C. Parisses, "A Novel Optimal PIλDND2N2 Controller Using Coyote Optimization Algorithm for an AVR System," *Engineering Science and Technology, an International Journal* 26 (2022): 100991.

41. M. Elsisi, "Design of Neural Network Predictive Controller Based on Imperialist Competitive Algorithm for Automatic Voltage Regulator," *Neural Computing and Applications* 31, no. 9 (2019): 5017–5027.

42. A. M. Mosaad, M. A. Attia, and A. Y. Abdelaziz, "Whale Optimization Algorithm to Tune PID and PIDA Controllers on AVR System," *Ain Shams Engineering Journal* 10, no. 4 (2019): 755–767.

43. D. Izci and S. Ekinci, "An Improved RUN Optimizer Based Real PID plus Second-order Derivative Controller Design as a Novel Method to Enhance Transient Response and Robustness of an Automatic Voltage Regulator," *e-Prime—Advances in Electrical Engineering, Electronics and Energy* 2 (2022): 100071.

17518652, 2025, 1, Downloaded from https://ietresearch.onlinelibrary.wiley.com/doi/10.1049/cth2.70068 by Bursa Uludag University Kutuphane ve Dokumantasyon, Wiley Online Library on [07/09/2026]. See the Terms and Conditions (https://onlinelibrary.wiley.com/terms-and-conditions) on Wiley Online Library for rules of use; OA articles are governed by the applicable Creative Commons License

44. A. Eltayeb, G. Ahmed, I. H. Imran, N. M. Alyazidi, and A. Abubaker, "Comparative Analysis: Fractional PID vs. PID Controllers for Robotic Arm Using Genetic Algorithm Optimization," *Automation* 5, no. 3 (2024): 230–245.

45. P. Gopi, S. V. Reddy, M. Bajaj, I. Zaitsev, and L. Prokop, "Performance and Robustness Analysis of V-Tiger PID Controller for Automatic Voltage Regulator," *Scientific Reports* 14, no. 1 (2024): 7867.

46. F. Dai and S. Gao, "Optimal Design of a PIDD2 Controller for an AVR System Using Hybrid Whale Optimization Algorithm," *IEEE Access* 12 (2024): 128525–128540.

47. M. S. Amin, M. A. Attia, et al., "Development of AVR Controller Performance Using Exponential Distribution and Transit Search Optimization Techniques," *Frontiers in Energy Research* 12 (2024).

48. B. Çavdar, E. Şahin, and E. Sesli, "On the Assessment of Meta-Heuristic Algorithms for Automatic Voltage Regulator System Controller Design: A Standardization Process," *Electrical Engineering* 106 (2024): 5801–5839.

49. A. K. Sahin, B. Cavdar, and M. S. Ayas, "An Adaptive Fractional Controller Design for Automatic Voltage Regulator System: Sigmoid-Based Fractional-Order PID Controller," *Neural Computing and Applications* 36, no. 23 (2024): 14409–14431.

50. A. Jegatheesh, V. Thiyagarajan, N. B. M. Selvan, and M. D. Raj, "Voltage Regulation and Stability Enhancement in AVR System Based on SOA-FOPID Controller," *Journal of Electrical Engineering & Technology* 19, no. 1 (2024): 31–44.

51. G. Saravanan, K. P. Suresh, C. Pazhanimuthu, and R. Senthil Kumar, "Artificial Rabbits Optimization Algorithm Based Tuning of PID Controller Parameters for Improving Voltage Profile in AVR System Using IoT," *e-Prime—Advances in Electrical Engineering, Electronics and Energy* 8 (2024): 100523.

52. A. Bouaddi, R. Rabeh, and M. Ferfra, "Optimal Control of Automatic Voltage Regulator System Using Hybrid PSO-GWO Algorithm-based PID Controller," *Bulletin of Electrical Engineering and Informatics* 13, no. 5 (2024): 3070–3080.

53. A. Sivanandhan and G. Thriveni, "Optimal Design of Controller for Automatic Voltage Regulator Performance Enhancement: A Survey," *Electrical Engineering* (2024).

54. R. Banerjee, A. Biswas, and J. Bera, "A Novel Integrated Differential-Routh Approach to Develop Reduced Order Controller With Improved Performance," *Electrical Engineering* 106, no. 3 (2024): 3001–3015.

55. Ö. Can and M. Ş. Ayas, "Fractional High-Order Differential Feedback Controller Based on Meta-Heuristic Algorithms for Automatic Voltage Regulator," *Electric Power Components and Systems* (2024): 1–14.

56. M. Silas and S. Bhusnur, "Upgradation of the Automatic Voltage Regulator Dynamic Response by an Optimally Tuned Fractional Order Controller," *International Journal of Modelling, Identification and Control* 44, no. 4 (2024): 328–340.

57. M. Č. Bošković, T. B. Šekara, D. M. Stojić, and M. R. Rapaić, "Novel Tuning Rules for PIDC Controllers in Automatic Voltage Regulation Systems Under Constraints on Robustness and Sensitivity to Measurement Noise," *International Journal of Electrical Power & Energy Systems* 157 (2024): 109791.

58. Ö. Türksoy and A. Türksoy, "A Fast and Robust Sliding Mode Controller for Automatic Voltage Regulators in Electrical Power Systems," *Engineering Science and Technology, an International Journal* 53 (2024): 101697.

59. N. D. Chetty, G. Sharma, R. Gandhi, and E. Çelik, "A Novel Salp Swarm Optimization Oriented 3-DOF-PIDA Controller Design for Automatic Voltage Regulator System," *IEEE Access* 12 (2024): 20181–20196.

60. Y. Hinislioglu and U. Guvenc, "A Novel Hyper-heuristic Algorithm: An Application to Automatic Voltage Regulator," *Neural Computing and Applications* 36 (2024): 21321–21364.

61. E. A. Mohamed, M. Aly, W. Alhosaini, and E. M. Ahmed, "Augmenting the Stability of Automatic Voltage Regulators Through Sophisticated Fractional-Order Controllers," *Fractal and Fractional* 8, no. 5 (2024): 300.

62. P. K. Pathak, M. Jain, and A. K. Yadav, "Metaheuristic-Assisted Advanced Control Approach for Time Delayed Unstable Automatic Voltage Regulator," *Electric Power Components and Systems* 52, no. 2 (2024): 173–188.

63. D. F. Zambrano-Gutierrez, G. H. Valencia-Rivera, J. G. Avina-Cervantes, I. Amaya, and J. M. Cruz-Duarte, "Designing Heuristic-Based Tuners for Fractional-Order PID Controllers in Automatic Voltage Regulator Systems Using a Hyper-Heuristic Approach," *Fractal and Fractional* 8, no. 4 (2024): 223.

64. A. Sabo, T. Ebuka Odoh, V. Veerasamy, and N. I. Abdul Wahab, "Modified Multimachine Power System Design With DFIG-WECS and Damping Controller," *Energies* 17, no. 8 (2024): 1841.

65. Z. Feng, W. Niu, and S. Liu, "Cooperation Search Algorithm: A Novel Metaheuristic Evolutionary Intelligence Algorithm for Numerical Optimization and Engineering Optimization Problems," *Applied Soft Computing* 98 (2021): 106734.

66. A. Tabak, "Maiden Application of Fractional Order PID plus Second Order Derivative Controller in Automatic Voltage Regulator," *International Transactions on Electrical Energy Systems* 31, no. 12 (2021): e13211.

67. Z. Long, J. Li, H. Yang, et al., "Methods and Experiments for Automatic Control of Surface Back Pressure Based on Dung Beetle Optimizer-PID Controller," *Process Safety and Environmental Protection* 191 (2024): 360–374.

68. Y. Li, W. Tan, and M. Yu, "Tuning Rules of Filtered PID/PIDD2 Controller for Integrating Processes With Measurement Noise," *International Journal of Systems Science* 55, no. 3 (2024): 467–481.

69. E. Çelik and M. Karayel, "Effective Speed Control of Brushless DC Motor Using Cascade 1PDf-PI Controller Tuned by Snake Optimizer," *Neural Computing and Applications* 36, no. 13 (2024): 7439–7454.

70. H. Su, D. Zhao, A. A. Heidari, et al., "RIME: A Physics-based Optimization," *Neurocomputing* 532 (2023): 183–214.

71. J. O. Agushaka, A. E. Ezugwu, and L. Abualigah, "Gazelle Optimization Algorithm: A Novel Nature-Inspired Metaheuristic Optimizer," *Neural Computing and Applications* 35 (2022): 4099–4131.

72. L. Wang, Q. Cao, Z. Zhang, S. Mirjalili, and W. Zhao, "Artificial Rabbits Optimization: A New Bio-inspired Meta-heuristic Algorithm for Solving Engineering Optimization Problems," *Engineering Applications of Artificial Intelligence* 114 (2022): 105082.

73. A. E. Ezugwu, J. O. Agushaka, L. Abualigah, S. Mirjalili, and A. H. Gandomi, "Prairie Dog Optimization Algorithm," *Neural Computing and Applications* 34, no. 22 (2022): 20017–20065.

74. I. Ahmadianfar, A. A. Heidari, A. H. Gandomi, X. Chu, and H. Chen, "RUN Beyond the Metaphor: An Efficient Optimization Algorithm Based on Runge Kutta Method," *Expert Systems with Applications* 181 (2021): 115079.

75. S. Li, H. Chen, M. Wang, A. A. Heidari, and S. Mirjalili, "Slime Mould Algorithm: A New Method for Stochastic Optimization," *Future Generation Computer Systems* 111 (2020): 300–323.

17518652, 2025, 1, Downloaded from https://ietresearch.onlinelibrary.wiley.com/doi/10.1049/cth2.70068 by Bursa Uludag University Kutuphane ve Dokumantasyon, Wiley Online Library on [07/09/2026]. See the Terms and Conditions (https://onlinelibrary.wiley.com/terms-and-conditions) on Wiley Online Library for rules of use; OA articles are governed by the applicable Creative Commons License

Appendix 1: MATLAB codes for ECSA-optimized RPIDD^2-PI controller-based AVR system.

```
% ECSA-based RPIDD2-PI controller
Ka = 10; Ta = 0.1; Ke = 1; Te = 0.4; Kg = 1; Tg = 1; Ks = 1; Ts = 0.01; % Nominal parameters of AVR
Kp1 = 3.8665; Ki1 = 0.74127; Kd1 = 1.3253; Kd2 = 0.11818; N1 = 1886.6; N2 = 1999.9; Kp2 = 1.3444; Ki2 = 0.28547; % Optimized
controller parameters
s = tf('s')
G = Ka*Ke*Kg/((s*Ta+1)*(s*Te+1)*(s*Tg+1)); H = Ks/(s*Ts+1);
C1 = Kp1+Ki1/s+Kd1*(N1/(1+N1/s))+Kd2*(N2/(1+N2/s))^2; C2 = Kp2+Ki2/s;
C = C1*C2;
T_ecsa = feedback(C*G, H);
t = 0:0.001:1; y_ecsa = step(T_ecsa, t); stepinfo(y_ecsa, t, 1)
plot(t, y_ecsa, t, 1+t*0)
legend('ECSA', 'Reference')
xlabel('Time (s)'); ylabel('Output voltage change (pu)')
```


17518652, 2025, 1, Downloaded from https://ietresearch.onlinelibrary.wiley.com/doi/10.1049/cth2.70068 by Bursa Uludag University Kutuphane ve Dokumantasyon, Wiley Online Library on [07/09/2026]. See the Terms and Conditions (https://onlinelibrary.wiley.com/terms-and-conditions) on Wiley Online Library for rules of use; OA articles are governed by the applicable Creative Commons License